LQCD-ext II

Computational Resources for Lattice QCD: 2015–2019

Revised, October 23, 2013

USQCD Collaboration Executive Committee

R. Brower, (Boston U.) N. Christ (Columbia U.), F. Karsch (BNL),
J. Kuti (UCSD), P. Mackenzie (Fermilab), J. Negele (MIT),
D. Richards (JLab), M. Savage (U. Washington), and R. Sugar (UCSB)

I. INTRODUCTION

For the past twelve years, the Department of Energy (DOE) has supported computational infrastructure for the numerical study of quantum chromodynamics (QCD) and other strongly coupled field theories. It has funded the development of software through four grants from the Scientific Discovery Through Advanced Computing (SciDAC) Program, the acquisition of dedicated hardware through the first of the SciDAC grants (SciDAC-1), the Lattice QCD Computing Project (LQCD), the current Lattice QCD Computing Project-ext (LQCD-ext), and a grant from the American Recovery and Reinvestment Act (LQCD ARRA). Current dedicated hardware consists of commodity clusters optimized for the study of lattice field theories, clusters with GPU and MIC accelerators, and a half-rack Blue Gene/Q. The operation of this hardware is supported through the LQCD-ext project. The software produced under the SciDAC grants is publicly available, and the dedicated hardware is open, on a peer reviewed basis, to all members of the USQCD Collaboration, which consists of nearly all of the high energy and nuclear physicists in the United States using the methods of lattice gauge theory. USQCD has also received major allocations on leadership class computers through the DOE's INCITE Program. The combination of access to leadership class computers, and our dedicated hardware, coupled with the SciDAC software effort, which has enabled highly efficient use of both, has made possible major progress in the established study of QCD and in the nascent field of strongly coupled beyond-the-standard-model (BSM) theories on the lattice , and helped to bring the field of lattice gauge theory to a point where it is now providing accurate determinations of a wide range of quantities of importance to experimental programs in high energy and nuclear physics.

The LQCD-ext Program runs through the end of fiscal year 2014. If the US QCD/BSM community is to exploit the enormous physics opportunities for lattice calculations outlined below and to remain internationally competitive, it must continue to renew its computational infrastructure well beyond that date. Therefore, in this proposal, we set out a plan for the acquisition and operation of dedicated hardware for the fiscal years 2015–2019. We note that our two current SciDAC grants, *Searching for Physics Beyond the standard model: Strongly Coupled Field Theories at the Intensity and Energy Frontiers* and *Computing Properties of Hadrons, Nuclear and Nuclear Matter from Quantum Chromodynamics*, run through the end of fiscal years 2015 and 2017, respectively, and will therefore be able to provide initial

software support for the proposed LQCD-ext II Project. We plan to request their renewals at the appropriate time, as well as the renewal of our current INCITE grant. The extension of all three components of our infrastructure effort is vital to its success.

In Section II of this document we set out our scientific objectives for the period 2015–2019, and indicate the potential impact of achieving them on DOE's experimental programs in high energy and nuclear physics. Work will focus on determination of the fundamental parameters of the standard model and the search for evidence of beyond-the-standard-model physics in hadrons; the study of strongly interacting matter under extreme conditions of temperature and density; the calculation of the masses, internal structure and interactions of strongly interacting particles; and the exploration of strongly coupled field theories that go beyond the standard model. In Section III we describe the computational resources needed from the DOE to achieve our scientific goals. They consist of a roughly equal mixture of cycles on the DOE's leadership class computers and on powerful dedicated hardware for capacity computing. The purpose of this proposal is to obtain the funds to acquire and operate the dedicated hardware, which we plan to locate at the three laboratories that have housed the LQCD, LQCD-ext and LQCD ARRA hardware: Brookhaven National Laboratory (BNL), Fermi National Accelerator Laboratory (FNAL), and Thomas Jefferson National Accelerator Facility (JLab). We request \$2.63M (\$2,630,000) per year for hardware acquisition, and an operations budget that starts at \$1.95M in 2015 and rises to \$2.18M in 2019. In Section IV we discuss the role of the USQCD Collaboration, and explain the processes by which it sets scientific priorities and allocates computational resources. We also describe the international collaborations in which members of USQCD are engaged, the sharing of large data sets through the International Lattice Data Grid (ILDG), and the software created under our SciDAC grants. In Section V we discuss the role of the participating laboratories, and in Section VI we set out the proposed management structure for LQCD-ext II.

II. SCIENTIFIC OBJECTIVES

The objective of LQCD-ext II is to enable numerical studies of QCD and BSM theories of the breadth and precision needed to have an important impact on the fields of high energy and nuclear physics. The required level of precision has been achieved for several quantities, and tools have been developed to do so for a wide range of others. Indeed, as the quality of lattice-QCD results and methodology has improved, more experimental programs look to these calculations to interpret their data and help conceive next-generation experiments.

The USQCD Collaboration [1] has spelled out the status and prospects for lattice gauge theory in four white papers, *Lattice QCD at the Intensity Frontier* [2], *Computational Challenges in QCD Thermodynamics* [3], *Lattice QCD for Cold Nuclear Physics* [4], and *Lattice Gauge Theories at the Energy Frontier* [5]. In this section, we draw from the material in these white papers to provide the baseline physics program of LQCD-ext II. As discussed in Sec. IV, the USQCD Collaboration has processes in place for evolving the science program as new experimental results and computing capabilities become available.

Before delving into details of the physics program of LQCD-ext II, it is instructive to take stock of the progress in validating lattice-QCD methodology. An *ab initio* understanding

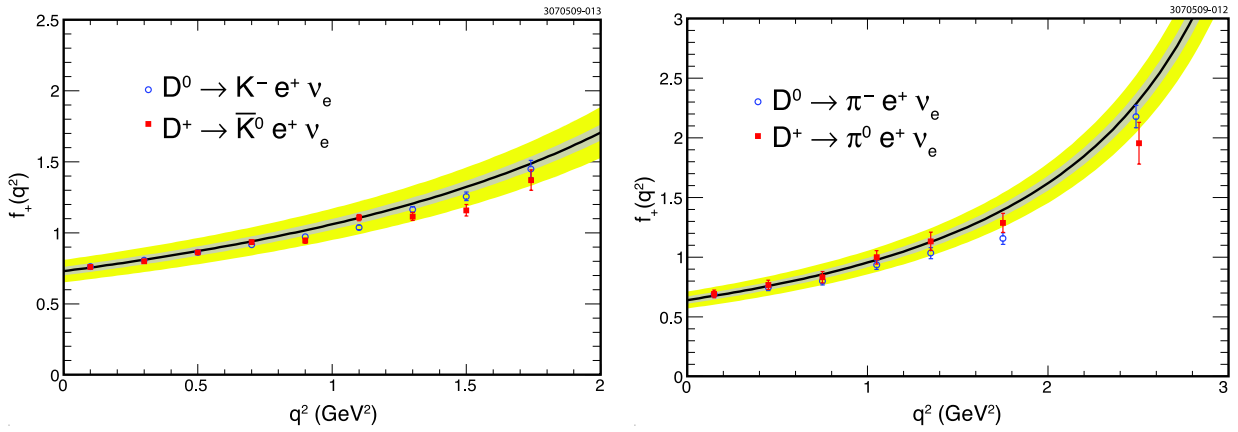

FIG. 1: Comparison [12] of $2+1$ lattice-QCD calculations of D-meson form factors [8, 11] (curves with error bands) with measurements from CLEO-c [12] (points with error bars).

of hadron masses was one of the original attractions of lattice QCD. In the last decade, the masses of many nucleons have now been calculated with high precisions and very good agreement with experiment. The mass of the nucleon, the source of everyday mass, has now been calculated with 1–2% accuracy [6]. The light hadron masses are *post*dictions, coming long after the experimental measurements were made, and many nuclear and particle physicists have wanted to see genuine predictions, which precede experiment. In work enabled by the LQCD and LQCD-ext infrastructure projects, USQCD groups computed charmed-meson decay constants [7], semileptonic form factors [8], and the masses of the B_c [9] and η_b [10] mesons before these quantities were measured in experiments that confirmed the computations. The charmed-meson semileptonic form factors are especially noteworthy, because they predict not only the normalization of the decay, but also the kinematic distribution. As shown in Fig. 1, these predictions have stood the test of time [8, 11, 12].

Lattice QCD calculations have also made progress in supplying results that cannot be obtained by any other means. A noteworthy development of the past decade lies in the determination of the QCD coupling α_s and the quark masses. These quantities are the fundamental parameters of QCD; the Lagrangian of lattice gauge theory contains free parameters corresponding to each one of them. To fix these bare parameters, $1+n_f$ hadronic quantities must be taken from experiment; this step is necessary and no different from any other formulation of QCD. The most recent Particle Data Group (PDG) Review [13] contains reviews on QCD [14] and on quark masses [15]. In the case of α_s, m_b, and m_c the lattice-QCD determinations [16–21] are now considered to be competitive with, and perhaps slightly superior to, determinations from high-energy scattering and decay processes, which are analyzed with perturbative QCD. Lattice QCD is the only way to determine the light-quark masses, m_s, m_d, and m_u with any meaningful precision. Before lattice QCD brought the errors under control, the quoted uncertainty on the strange quark mass was approximately 30% and it was not clear whether the up quark mass was consistent with zero or not. Now several lattice-QCD calculations have controlled most of the dominant uncertainties [22–25], to accuracies of a few per cent [15]. Importantly, they have shown that the mass of the up quark is nonvanishing, a result of profound significance for the solution of the strong CP problem.

In nuclear physics, lattice QCD has provided a wealth of information on the transition to a phase in which quarks lose confinement. Several years ago, we found that the transition

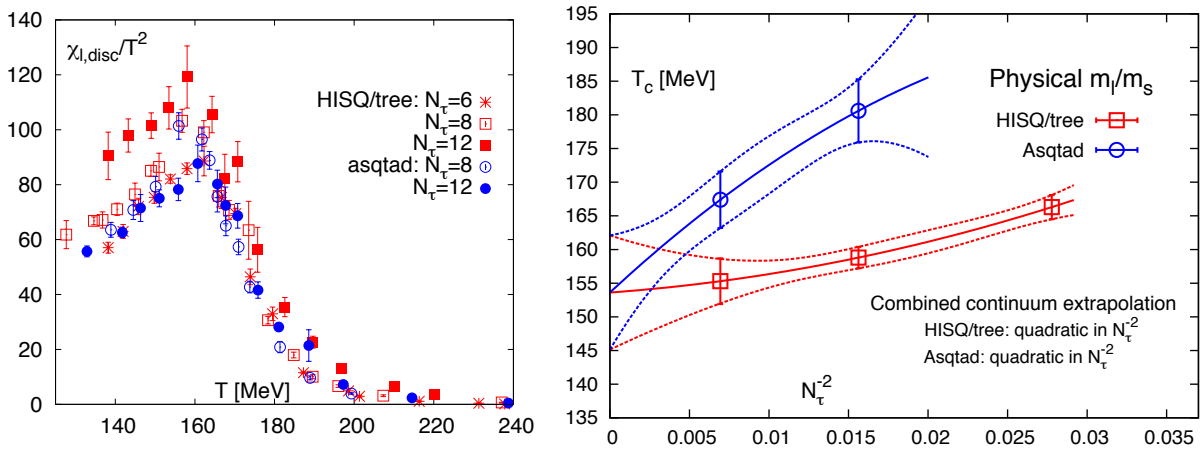

FIG. 2: The peak in the chiral susceptibility with two different actions and several lattice spacings (left). The peak positions are plotted vs. lattice spacing squared (right) to obtain the transition temperature, $T_c = 154(9)$ MeV, in the continuum limit [26]. This temperature agrees with the results of other lattice-QCD groups [27, 28].

is a smooth crossover, which changed our understanding of how the early universe cooled. Remarkably, the quark masses, though small, are just large enough to cause this behavior. During LQCD-ext, the transition temperature has been identified by calculating the peak position of the relevant susceptibility, as shown in Fig. 2. The present 6% precision is enough to aid the analysis of quark-gluon plasma at RHIC.

Another important goal in nuclear physics is building a three-dimensional image of the nucleon. Here we explore the role of quark and gluon orbital angular momentum, inspired by the experimental program at Jefferson Lab in the U.S. and elsewhere around the world. These experiments constrained the total angular momentum carried by the u and d quarks, while lattice QCD provided *ab initio* values for the total orbital angular momentum. To obtain a full understanding, however, we will need a further round of QCD calculations, enabled by LQCD-ext II, which will be compared with new measurements in the 12-GeV JLab program [29].

A. The Intensity Frontier

One of the foremost goals of high-energy physics is to test the standard model of particle physics (SM) and thereby search for indications of new physics beyond. Quark-flavor experiments at the intensity frontier have historically played a key role, because their natural reach can far exceed that directly probed in colliders, in some cases as high as 1,000 TeV or even 10,000 TeV [30]. During the coming decade, quark-flavor experiments will continue both at e^+e^- machines (BES III near the charm threshold, and Belle II at the $b\bar{b}$ threshold) and the LHC, which has a dedicated b- and c-quark experiment, LHCb, as well as some b physics in the central detectors ATLAS and CMS. Furthermore, a new set of kaon experiments is being mounted: NA62 at CERN, KOTO at J-PARC, and the proposed ORKA experiment at Fermilab. To interpret these experiments, one often requires lattice-QCD calculations of hadronic properties. Thus, LQCD infrastructure has been and will be an essential theoretical adjunct to the experimental high-energy physics program.

Other experiments at the intensity frontier will depend critically on the LQCD-ext II infrastructure proposed here. The Muon $g-2$ Experiment at Fermilab expects a four-fold reduction in the experimental uncertainty of the muon magnetic moment. The leading theoretical uncertainties, stemming from hadronic contributions to $g-2$, will dominate the total uncertainty unless they are improved. Lattice QCD offers the only feasible path to a controlled theoretical error. Matrix elements of protons and neutrons are needed to interpret constraints on CP violation from limits on electric dipole moments, to interpret possible muon-to-electron conversion events in terms of new physics models, to disentangle sources of uncertainty in neutrino quasi-elastic scattering, to aid the search for baryon-number violation in proton decay and neutron-antineutron oscillations, and also to guide searches for dark matter and axions at the cosmic frontier. With the resources proposed here, the USQCD Collaboration will be able to expand its program to meet the needs of these and other upcoming intensity-frontier experiments.

1. Quark flavor physics

In the 2008 proposal for LQCD-ext, we argued that the stage was set for a rapid maturation of calculations of electroweak matrix elements. At that time, the era of precision lattice-QCD calculations was just beginning. Lattice-QCD methods had been validated at the few percent level for a range of spectroscopic quantities [31], and accurate results were available for f_π (2.6% error), f_K (2.0% error), and f_K/f_π ($\sim$ 1% error) using improved staggered fermions [32]. For other quantities, first unquenched calculations were available, but some errors were not fully controlled. In addition, cross-checks from using multiple fermion discretizations were not yet available.

With the LQCD-ext hardware, resources on leadership-class supercomputers, SciDAC support for software, and junior physicists entering the field, the present situation is vastly better. Results with fully controlled errors are available for nearly 20 matrix elements, in almost all cases with multiple independent calculations. Errors have been steadily reduced, such that sub-percent level is now possible for some of them. One indication of the maturation of calculations is that it is now appropriate to perform world averages of lattice-QCD results, so as to provide the best input for phenomenological analyses [33, 34].

The amplitudes listed so far all have one hadron in the initial state and zero or one in the final state and are, thus, especially straightforward. Nonleptonic decays such as $K \to \pi\pi$ are more challenging. In 2008, we argued that sustained, continuing support for lattice QCD would allow us to bring these kinds of calculations under control too. Indeed, in 2012 the amplitude for $I = 2$ was brought under control [35, 36], and we are making progress on the $I = 0$ amplitude [37] and the long-distance contribution to ΔM_K [38].

In Table I, we demonstrate this progress quantitatively for twelve of the most important quantities. We compare lattice errors in various matrix elements to those in the corresponding experimental measurements, and, where available, we include (quite accurate) forecasts made in 2007 [31] for the errors expected in 2012-2013. The new set of forecasts are explained in detail in the USQCD white paper *Lattice QCD at the Intensity Frontier* [2].

Since 2007, calculations of all quantities in Table I have, as for f_K/f_π, brought all errors under control. Often multiple calculations with different fermion discretizations are available. For

TABLE I: History, status, and future of selected lattice-QCD calculations needed for the determination of CKM matrix elements. Forecasts from the 2008 LQCD-ext proposal (where available) assumed computational resources of 10–50 TF years. Most present lattice results are taken from latticeaverages.org [33]. Other entries are discussed in the text. The quantity $\xi = f_{B_s} B_{B_s}^{1/2} / f_B B_B^{1/2}$.

Quantity	CKM element	Present expt. error	2007 forecast lattice error	Present lattice error	2018 lattice error
f_K/f_π	$\lvert V_{us}\rvert$	0.2%	0.5%	0.5%	0.15%
$f_+^{K\pi}(0)$	$\lvert V_{us}\rvert$	0.2%	–	0.5%	0.2%
f_D	$\lvert V_{cd}\rvert$	4.3%	5%	2%	$< 1\%$
f_{D_s}	$\lvert V_{cs}\rvert$	2.1%	5%	2%	$< 1\%$
$D \to \pi\ell\nu$	$\lvert V_{cd}\rvert$	2.6%	–	4.4%	2%
$D \to K\ell\nu$	$\lvert V_{cs}\rvert$	1.1%	–	2.5%	1%
$B \to D^*\ell\nu$	$\lvert V_{cb}\rvert$	1.3%	–	1.8%	$< 1\%$
$B \to \pi\ell\nu$	$\lvert V_{ub}\rvert$	4.1%	–	8.7%	2%
f_B	$\lvert V_{ub}\rvert$	9%	–	2.5%	$< 1\%$
ξ	$\lvert V_{ts}/V_{td}\rvert$	0.4%	2-4%	4%	$< 1\%$
ΔM_s	$\lvert V_{ts}V_{tb}\rvert^2$	0.24%	7–12%	11%	5%
B_K	$\mathrm{Im}(V_{td}^2)$	0.5%	3.5–6%	1.3%	$< 1\%$

$B \to D^{(*)}$ form factors and f_B, lattice errors are at, or below, the level of the corresponding experimental errors. First row unitarity, which relies on lattice results for f_K/f_π and the $K \to \pi\ell\nu$ form factor, is seen to hold at the part-per-mille level [34, 39, 40]. In general, the CKM paradigm describes experimental observations at the few-percent level, while in detail the improved precision has unearthed a tension of around 3σ in the global fit [41]. USQCD calculations have played the major role in these developments. For example, the world average for B_K is based on four different calculations, three of which were carried out under the auspices of USQCD.

We describe now a broad program of intensity-frontier calculations that will be possible with LQCD-ext II. We have organized this program according to physics topic or class of experiments for which the calculations are needed. In each component, we explain the physics goals and their relationship to the experimental program, describe the status of present lattice-QCD calculations, and explain what can be achieved over the next five years.

While the challenges to further reductions in errors depend on the quantity, there are many common features. A key advance over the next five years will be the widespread simulation using physical u and d quark masses, obviating the need for chiral extrapolations. A second advance will be the systematic inclusion of isospin-breaking and electromagnetic (EM) effects. A third across-the-board improvement that will likely become standard over the next five years is the use of charmed sea quarks.

Let us begin with a discussion of the next generation of calculations for the *standard matrix elements* listed in Table I. Although they are already mature, we can significantly tighten constraints on the SM by improving these calculations, with the aim of reducing, and ultimately removing, the gap between lattice and experimental errors. Key improvements to all quantities come particularly from the use of physical quark masses, finer lattice spacings,

improved lattice actions, and (in some cases) higher statistics.

- **$B \to D^{(*)}$ form factors**, which allow for the determination of $|V_{cb}|$. The lattice-QCD errors now approach and during LQCD-ext II are expected to drop below the experimental error. The form factors also pertain to new physics in $B \to D^{(*)}\tau\nu$, which exceed existing SM predictions by a combined (D and D^* modes) 3.2–3.4σ [42, 43]. Measurements of the decay rates by BaBar and Belle will be improved by Belle II. The parametric error in $|V_{cb}|$ is the dominant uncertainty in the current standard model estimates for $K^+ \to \pi^+\nu\bar{\nu}$ and $K_L \to \pi^0\nu\bar{\nu}$ decay rates, but will be below the error from a thousand-event experiment with the projected improvements.

- **$B \to \pi$ form factors**, which provide the primary method of determining $|V_{ub}|$. While present lattice errors are about double those of experiment, we forecast a halving of the former by 2014 and a further halving by 2018. Measurements of the decay rate by BaBar and Belle will be improved by Belle II.

- **B-meson decay constants and mixing parameters**, which provide further constraints on the unitarity triangle. Recently, lattice errors on D-meson decay constants have reached $\sim 1\%$ errors using relativistic light-quark methods with automatically normalized vector and axial currents. Toward the middle of the LQCD-ext II era, increases in computational resources will allow small-enough lattice spacings to apply this technique to b-quarks. Measurements of the leptonic decay rate will be improved by Belle II; measurements of the oscillation frequencies will be improved by LHCb.

- **f_K/f_π and $f_+^{K\pi}(0)$**, which constrain first-row CKM unitarity. Despite the current 0.5% errors, experimental errors are smaller still.

Finally, we note that, for a few quantities, there is little impetus for improvement in the short term. Most notable is $\hat{B}_K$, where percent-level accuracy has been achieved through a concerted worldwide effort, with thorough cross checks.

With this foundation, there are several *straightforward extensions* employing the same techniques but with a keener focus on BSM physics.

- **BSM contributions to K-, D-, and B-meson mixing and $\Delta\Gamma_B$.** For each of the K, D and B systems there are four new matrix elements, in addition to the one in the SM, for any BSM extension. The calculations are straightforward generalizations of the SM case and are already underway [44–46]. Results of comparable accuracy to those already obtained for the corresponding SM matrix elements should be available by 2014.

- **$B \to K\ell^+\ell^-$ and related penguin decays.** These processes probe new physics, assuming one has the vector, scalar, and tensor form factors. $B \to K\ell^+\ell^-$, $B \to K^*\ell^+\ell^-$ and $B \to K^*\gamma$ are now well measured in experiment, and increasingly accurate results are expected over the coming five years from both LHCb and Belle II. During the same time frame searches for $B \to \pi\ell^+\ell^-$, $K \to \pi\ell^+\ell^-$, $\Lambda_b \to \Lambda_c\ell^+\ell^-$, and $B_s \to \phi\gamma$ will be carried out. Calculations are underway for some of these modes [47–49], and more are planned.

The matrix elements discussed in these two lists have at most one hadron in the final state. With recent advances, it is now possible to carry out calculations with two hadrons in the final state. The proposed LQCD-ext II hardware infrastructure will allow further exploration of such processes. In all these cases, rescattering effects introduce finite-volume distortions, which can be corrected in a nonperturbative manner in principle [50, 51] and in practice [52, 53].

- **The $\Delta I = 1/2$ rule**, which is the dominance of the $I = 0$ amplitude A_0 over $I = 2$ in $K \to \pi\pi$ decay. The complex $I = 2$ amplitude A_2 has now been computed using DWF with 15% errors [35, 36] and, in the next two years, the dominant discretization error will be reduced, leading to a total error of $\sim 5\%$. The $I = 0$ amplitude is considerably more challenging [54], so first physical results for A_0 with 15% errors are expected by 2014, and a 10% error appears possible by 2018.
- **Kaon ε'/ε**, which is the measure of direct CP violation in the neutral kaon system. The major source of uncertainty in ε' stems from A_0, so the forecast is again 15% errors by 2014 and 10% by 2018. With this precision, existing measurements from KTeV and NA48 can be used to constrain new physics.
- **Long-distance contributions from charm-quark loops.** In several processes, long-distance contributions from charm-quark loops can pose a problem, because large higher-orders corrections can appear when charm is treated perturbatively [55]. Treating charm loops within lattice QCD would eliminate the problem. An example is ΔM_K, for which work is in progress [38]. These effects enter at some level in the decays $K^+ \to \pi^+\nu\bar{\nu}$, $K_L \to \pi^0\nu\bar{\nu}$, and $K \to \pi\ell^+\ell^-$, which are a focus of the coming decade's experimental program.

Finally, let us mention that there is much interest in nonleptonic D-meson decays. They differ from $K \to \pi\pi$ in that there are many final states that can rescatter into each other [56]. This topic is a challenging line of research that LQCD-ext II will stimulate.

2. Muon anomalous magnetic moment

The muon anomalous magnetic moment provides one of the most precise tests of the standard model of particle physics (SM) and often places important constraints on new theories beyond the SM [57]. The current discrepancy between experiment and the standard model has been reported in the range of 2.9–3.6 standard deviations [58–60]. With new experiments planned at Fermilab (E989) and J-PARC (E34) that aim to improve on the current 0.54 ppm measurement at BNL [61] by a factor of four (0.14 ppm or better), it will continue to play a central role in particle physics in the coming decade.

The hadronic corrections to $a_\mu = (g-2)/2$ are the largest source of error in the SM calculation. They enter at order α^2 through the hadronic vacuum polarization (HVP), and α^3 through hadronic light-by-light (HLbL) scattering. We discuss their status in turn, emphasizing how lattice QCD can leverage the new experiment, as desired [57].

The HVP contribution to the muon anomaly has been obtained with 0.6% accuracy (0.36 ppm of $g-2$) from experimental measurements of $e^+e^- \to$ hadrons and $\tau \to$ hadrons [59,

60], but the two results disagree at the 2σ level [59]. Lattice-QCD calculations enabled by LQCD-ext II will provide an important independent check. At the moment statistical errors on lattice calculations of a_μ(HVP) are at about the 3–5% level [62–67]. Important systematic errors remain, which are being addressed [67–70]. To get to the 1% level, or better, disconnected diagrams and isospin breaking effects must be incorporated, which will require the resources of the second half of the LQCD-ext II program.

The HLbL contribution cannot be usefully related to experimental data. Present estimates are based on models of QCD and estimate errors in the 25–40% range [71, 72], a contribution of 0.22-0.35 ppm of $g-2$. Thus, an *ab initio* calculation is crucial, and the lack thereof has been used as a reason not to do the new experiment. Fortunately, significant progress has been made with lattice QCD, and the prospects for achieving a calculation with $\sim 20\%$ errors in the next five years are good. Our longer-term ambitious goal, which is not guaranteed, is to reduce the HLbL error to 10% by the end of LQCD-ext II[73], at which point the theoretical uncertainty will be lower than the projected experimental error.

3. Muon-to-electron conversion

In the standard model with neutrino masses and mixing, charged-lepton flavor violation is possible, but unobservable small. Thus, any observation of $\mu N \to eN$, where N is a nucleus, or the related process $\mu \to e\gamma$ would be an unambiguous sign of new physics. Many experiments searching for charged-lepton flavor violation are running or are on the horizon, for example the Mu2e Experiment at Fermilab, which aims to reduce the sensitivity to $\mu N \to eN$ by four orders of magnitude.

To interpret these experiments, lattice-QCD calculations of the light- and strange-quark contents of the nucleon are needed [74, 75]. These are the matrix elements $\sigma_{\pi N} = \frac{1}{2}(m_u + m_d)\langle N|(\bar{u}u + \bar{d}d)|N\rangle$, $m_s\langle N|\bar{s}s|N\rangle$, and the ratio $\langle N|(\bar{u}u - \bar{d}d)|N\rangle/\langle N|(\bar{u}u + \bar{d}d)|N\rangle$. These matrix elements are noiser than for meson analogs, and, as isoscalar operators, require disconnected diagrams. Still, many lattice collaborations have calculated the strange-quark content $m_s\langle N|\bar{s}s|N\rangle$ with $N_f = 2+1$ and even $N_f = 2+1+1$ flavors [76–85]. The results obtained with different fermion formulations agree at the 1–2σ level: a recent compilation quotes an average value $m_s\langle N|\bar{s}s|N\rangle = 40 \pm 10$ MeV [85]. Lattice-QCD can also provide first-principles calculations of the pion-nucleon sigma term $\sigma_{\pi N}$ [76, 78–80, 84] and the charm-quark content $m_c\langle N|\bar{c}c|N\rangle$ [83, 86]. A realistic goal for the next five years is to pin down the values of the quark scalar densities for $q = u, d, s, c$ with $\sim$ 10–20% uncertainties. Even greater precision can be expected on the timescale of a continuation of Mu2e.

4. Neutrino physics

Neutrino experiments—from the upcoming NOvA and MINOS+ to future projects such as LBNE and neutrino factories—are expected to play a central role in US particle physics. Measurement of neutrino oscillation parameters, and the possible discovery of new neutrino states, is limited by our understanding of the cross section at accelerator energies. The basic signal process is charged-current quasi-elastic (CCQE) scattering on a bound neutron. It is described by the axial-vector form factor of the nucleon, $F_A(q^2)$, which is related to the matrix element $\langle p|\bar{u}\gamma^\mu\gamma^5 d|n\rangle$. Usually, the q^2 dependence is modeled by a dipole form [87]

but this description is known to be inadequate in the related process of electron-nucleon scattering [88]. Uncertainty from this model of the form factor translates into an uncertainty of around 40% in the CCQE cross section [89–92], different experiments are not in good agreement for the single parameter in the dipole Ansatz. The discrepancies could originate from nuclear effects in the target, but without an *ab initio* understanding of the nucleon-level form factor, one cannot know.

The shape of the axial-vector form factor $F_A(q^2)$ can be calculated from first principles with lattice QCD. Worldwide, a significant, ongoing effort is devoted to calculating $F_A(Q^2)$ [93–96]. Until recently, results for the axial charge $g_A = F_A(0)$ have unfortunately not agreed well with neutron β decay experiments. Now, however, two papers [97, 98] find results in agreement with experiment, $g_A \approx 1.22$–1.24. Once they have been confirmed, and other checks are successful, we should be able to determine the shape reliably.

The current status of neutrino-nucleon scattering sets two interesting targets for the desired uncertainty in a lattice-QCD calculation of the form factor's slope. One is 12–25%, which is the uncertainty from model-independent fits to the MiniBooNE data [90]. The other is 5%, the putative uncertainty from the dipole fits. Refs. [97, 98] report total errors (apart from the omission of the strange and charmed sea) of a few per cent. Their work suggests that both phenomenologically relevant targets can be reached with the gauge-field ensembles proposed here.

Also important for neutrino scattering is neutral-current elastic scattering. The physics issues run parallel to those discussed here, but now we must calculate an isoscalar matrix element with lattice QCD. The resulting disconnected diagrams make the calculations noisier and costlier, so we forecast a more modest precision of $\sim 20\%$.

5. Other nucleon matrix elements

Grand-unified theories predict proton decay and neutron-antineutron mixing. A small-scale effort has been devoted to these calculations, leading to errors of $\sim 20\%$ [99, 100]. It should be straightforward to reduce these errors to the $\sim 10\%$ level during LQCD-ext II. Future underground neutrino detectors such as the proposed third phase of LBNE will improve limits on the proton lifetime. Similar matrix elements are also important for CP-violating electric dipole moments [101, 102], for axion [82, 103, 104] and dark matter [77, 82, 83, 85] searches. Higgs-mediated dark matter interactions require the same matrix elements as muon-to-electron conversion.

6. Precision Higgs Physics: the heavy quark masses and α_s

The fundamental parameters of QCD—α_s and the quark masses—are by-products of previously discussed phenomenological calculations. Lattice QCD calculations are currently the most precise method for obtaining all of these except m_b (and m_t, for which lattice QCD is not needed). For m_b, lattice calculations will eventually produce the most precise results. Lattice QCD is the only first principles method for obtaining the light quark masses, m_u, m_d, and m_s.

The heavy quark masses are of great importance for future high-precision Higgs studies. Future colliders aim to study Higgs branching fractions to 1% accuracies [105, 106]. The

Higgs partial width to its dominant decay channel is proportional to m_b^2. In order that the branching fraction uncertainties not be dominated by parametric uncertainty, m_b must be known to $\ll 0.5\%$. This is achievable with lattice QCD, but probably not with any other method. The most precise methods for obtaining the heavy quark masses, either with lattice QCD [20, 107] or without [108], employ correlation functions of heavy-quark bilinears. The moments of these have been calculated to third order in QCD perturbation theory. The perturbative expressions can be fit to moments of the heavy-quark e^+e^- production cross section, yielding the most precise results for m_c and m_b obtainable without lattice QCD. These correlation functions can also be calculated directly from lattice QCD much more accurately than they can be determined from e^+e^- experiment. The precision stands at 0.5% and 0.6% for m_c and m_b, respectively. The error for m_c is dominated by continuum perturbative QCD [20] so it cannot be improved with lattice gauge theory alone. On the other hand, statistics and discretization effects dominate the error in m_b. We expect to halve the error on m_b with the resources proposed here. Eventually, the best results for both m_c and m_b will come from lattice QCD.

7. Resources for Studies at the Intensity Frontier

To close this section, we discuss the computational resources needed to reach the scientific goals in quark flavor physics. As in the past, our work at the intensity frontier is envisioned to focus on two formulations of sea quarks: domain-wall fermions (DWF) [109–111], and highly improved staggered quarks (HISQ) [112]. Each of these formulations has its own compelling advantages. Furthermore, at the aimed-for precision, it will be very useful to employ two formulations for a healthy subset of the work in order to make certain that

No.	N_f	a(fm)	$N_s \times N_t$	Time units	TF years (configs.)	TF years (meas.)
#1	2+1	0.110	$48^3 \times 96$	2,500	90	60
#2	2+1	0.086	$64^3 \times 128$	2,500	95	70
#3	2+1+G	0.144	$32^3 \times 64$	4,000	90	50
#4	1+1+1+QED	0.110	$48^3 \times 96$	2,500	130	90
#5	1+1+1+QED	0.086	$64^3 \times 128$	2,500	145	100
#6	2+1	0.057	$96^3 \times 192$	1,800	320	220
#7	2+1+1	0.057	$96^3 \times 192$	1,800	320	220
#8	2+1+1	0.043	$128^3 \times 256$	1,400	1,050	750
Total DWF intensity frontier resource estimate						3,800

TABLE II: Resources to generate gauge configurations and perform important measurements with domain-wall fermions. The flavor notation is intended to be self-explanatory. For example, "2+1+1" indicates that the simulation masses of the up and down quark are equal and that strange and charmed sea quarks are also included. The combination "1+1+1" indicates unequal up and down quark masses and only a dynamical strange quark. Ensembles with +QED in the N_f column include dynamical photon fields while +G indicates imposed G-parity boundary conditions. The measurements determine the meson spectrum, pseudoscalar decay constants, $K \to \pi\pi$ decay amplitudes (A_0 in run #3 and A_2 for the others) and $Kl3$ form factors.

N_f	a (fm)	m_u/m_d	$N_s^3 \times N_t$	Configuration generation (TF years)	Pseudoscalar measurements (TF years)
2+1+1	0.060	1.00	$96^3 \times 192$	14	24
2+1+1	0.045	1.00	$128^3 \times 256$	72	100
2+1+1	0.030	1.00	$192^3 \times 384$	650	760
1+1+1+1+QED	0.060	0.44	$96^3 \times 192$	32	56
1+1+1+1+QED	0.045	0.44	$128^3 \times 256$	170	240
Total HISQ intensity frontier resource estimate					2,118

TABLE III: Resources to generate gauge configuration ensembles with four flavors of HISQ quarks. Notation as in Table II; 1+1+1+1 indicates that all four quark masses are unequal. The fifth and sixth column give the resources in TF years for 6,000 molecular dynamics time units (1,000 equilibrated gauge configurations).

systematic errors are truly under control.

The ensembles proposed here enjoy several qualitative advantages over their predecessors. All ensembles now have physical light quark masses, namely $m_\ell = (m_u + m_d)/2$; some of the planned HISQ ensembles even have $m_u \neq m_d$ with both tuned to their physical values. To tame concomitant finite-volume effects, all (with one exception) box sizes are (approximately) 6 fm on a side, with twice the time extent. Some of the DWF ensembles and all of the HISQ ensembles simulate charmed sea quarks. Finally, some planned ensembles will contain dynamical QED photon fields together with the QCD gluon fields. As the foregoing discussion makes clear, all these features are necessary to meet the aims of the intensity-frontier program.

The computational resources needed for our calculations with the DWF and HISQ actions are shown in Tables II and III, respectively. We report the estimated resources in teraflop-years (TF years).[1] The estimates are based on current algorithms and, thus, may well turn out to be conservative.

In summary, the future success of intensity-frontier research hinges on reliable SM predictions on the same time scale as the experiments and with commensurate uncertainties. Many of these SM predictions require nonperturbative hadronic matrix elements that can only be computed numerically with lattice QCD. Given the track record of our forecasts, cf. Table I, one can see that we are on track to make continued major contributions, if this proposal is funded.

[1] One TF-Year is defined to be the number of floating points operations produced in one year by a computer that sustains one teraflop/s. Unless stated otherwise, sustained performance is measured as the average of that sustained by the sparse matrix inversion routines for computing the quark propagators for the Domain Wall and improved Staggered (asqtad/HISQ) quark actions under production conditions.

B. The structure, spectrum and interactions of Hadrons

The strong interaction described by QCD is responsible for a diverse range of physical phenomena, including binding gluons and the lightest quarks into hadrons such as protons and neutrons, and through its manifestation as the strong nuclear force, it then binds neutrons and protons together to form the elements of the periodic table. Thus QCD is the cornerstone of nuclear physics, and the next five years will be a transformational period. The 12 GeV upgrade of Jefferson Laboratory will explore the role of gluonic excitations in the spectrum, build a three-dimensional tomographic view of the proton, and through parity-violating electron scattering explore fundamental symmetries of the standard model. Experiments at RHIC-spin will probe the gluon and antiquark contributions to the spin of the proton, and experiments at JLab will explore the contribution of orbital angular momentum. The construction of the *Facility for Rare Isotope Beams* will enable the exploration of multi-nucleon interactions from neutron-rich nuclei. The lattice-QCD calculations described herein are essential to fully realize the potential of these facilities. Calculations of hadron structure will provide a far more complete three-dimensional mapping of the nucleon than experiment can alone. Calculations in spectroscopy will *predict* features of the meson spectrum before experiment. Calculations of the interactions between hadrons will refine the chiral two-, three-and four-nucleon, and more generally baryon, forces directly from QCD. Finally, calculations of hadronic contributions precision measurements, such as the muon g-2, are essential to reveal the underlying symmetries of the standard model and to search for physics beyond.

1. Hadron Structure

Just as calculating the structure of atoms was a cornerstone of quantum mechanics, a cornerstone of contemporary nuclear physics is to achieve a quantitative, predictive understanding of the structure of nucleons and other hadrons using lattice QCD. One goal is precision calculation of fundamental quantities characterizing the nucleon, including form factors, moments of parton densities, helicity, and transversity distributions, moments of generalized parton distributions (GPDs), and transverse momentum distributions. Hadronic observables calculated from first principles are directly relevant to experiments at JLab and RHIC-spin and will have significant impact on future experiments at the JLab 12 GeV upgrade and a planned electron-ion collider. Another goal is obtaining insight into how QCD works. How does the spin of the nucleon arise from the helicity and orbital angular momentum of quarks and of gluons? How does hadron structure change as one varies parameters that cannot be varied experimentally, such as the number of colors, the number of flavors, or the quark masses? Another goal is to aid in the search for physics beyond the standard model.

Electromagnetic form factors reveal the distribution of charge and current and how constituents interact to recoil together at high momentum transfer. The statistical error in current lattice calculations [113] of the isovector charge radius is comparable to the discrepancy between electron scattering and Lamb shift measurements, so future high precision calculations will be important in helping resolve this discrepancy. The axial charge, g_A, governing neutron β-decay, is the value of the axial form factor at zero momentum transfer. Precision calculation at a fraction of a percent will impact the proton-proton fusion rate central to solar models and constrain the weak matrix element $|V_{ud}|$. The scalar and tensor

charges, g_S and g_T, are essential in searching for physics beyond the standard model in ultra-cold neutron experiments at LANL. A precise prediction of the tensor charge will be particularly significant prior to a major experimental program to measure it at the Jlab 12 GeV upgrade.

Quark parton distributions, studied in deep-inelastic scattering experiments around the world, specify the quark density, spin, and transversity distributions as functions of the momentum fraction, x, of the struck quark. Chiral extrapolations of lattice calculations [95] of the lowest moment of the spin distribution agree with deep inelastic scattering results from HERMES [114] and show that only about 30% of the nucleon spin comes from quark spin. GPDs specify quark density, spin, and transversity as functions of both the longitudinal momentum fraction x and the transverse position, and if known completely would provide a 3-dimensional picture of the nucleon. Their lowest three moments in x can be calculated using lattice QCD, and the combination of these moments with convolutions of GPDs measured at JLab and elsewhere will provide a more complete understanding of GPDs than either effort could obtain separately. Of particular interest and relevance to the DOE nuclear physics experimental program is the fact that one combination of moments of GPDs specifies the total angular momentum of quarks in the nucleon [95, 115–117], so combined with the quark spin contribution above, the lattice can provide a complete determination of quark spin and orbital contributions to the total spin 1/2 of the nucleon.

For the next 5 years, the primary focus will be precision computation of form factors, moments of quark parton distributions, and moments of quark GPDs at the physical pion mass with control of systematic errors associated with finite lattice spacing, spatial volume, temporal extent and excited state contaminants. These calculations are explicitly required to meet the **2014 NSAC Performance Measure HP9** and address experimental measurements mandated by six of the other nine Performance Measures. They are essential for realizing the full physics potential of experiments at the JLab 12 GeV upgrade, RHIC-spin, and a planned electron-ion collider. Both domain wall and isotropic Wilson clover actions will be used, sharing configurations with spectroscopy, nuclei, and intensity frontier projects, refining the the quantification of discretization uncertainties. The chiral symmetry of domain wall fermions eliminates some operator mixing, while the computational economy of Wilson clover fermions facilitates calculation of systematic errors and disconnected diagrams.

The dominant contributions to nucleon observables are the so-called connected diagrams, and two cost estimates of their cost for the full suite of observables are given in Table IV. Column Str-A yields 3% precision for the minimally demanding quantity g_A, with the other observables generally having larger errors. The entries in column Str-B denoted by † yield 3% precision for the maximally demanding quantity $\langle x \rangle$, with the other observables generally having smaller errors. The smaller contributions of disconnected diagrams, though much more computationally demanding, are essential for precision calculations of properties of protons and neutrons separately. If additional resources beyond Moore's law projections become available, we would add some of the following: form factors at high momentum transfer, higher moments of quark structure functions, gluon contributions to nucleon observables, and transverse momentum distributions.

2. Hadron Spectroscopy

The calculation of the bound state spectrum of QCD encapsulates our ability to describe the strong interactions, and the confrontation of high-precision calculations with experimental measurements will provide verification of the theoretical framework. Experimental investigation of the excited states of QCD has undergone a resurgence: the observation of new states in the charmonium system at Belle and at BaBar, the search for the so-called missing baryon resonances of the quark model at CLAS at JLab@6GeV, and the flagship search for so-called exotic mesons, states that must possess a richer structure than a quark-antiquark pair with relative angular momentum, at GlueX at the upgraded JLab@12GeV. How do the apparent collective degrees of freedom arise that describe the spectrum arise, and can we identify them? What role do gluons play in the spectrum, and how are they manifest? The work proposed here will facilitate those calculations both to describe the existing experimental data, and to *predict* the outcomes of future experiments.

Calculations of the spectrum are already profoundly impacting our understanding of QCD. Those of isovector and isoscalar mesons suggest exotics in a regime accessible to GlueX, and the presence of non-exotic "hybrids" where the gluons play an essential rôle. Those of the nucleon and Δ excited baryon spectrum[118] exhibit a counting of levels consistent with the non-relativistic qqq constituent quark model and inconsistent with a quark-diquark picture of baryon structure, and suggest the presence of "hybrid" baryons where the gluonic field plays a vital structure role. The excited-state spectrum is characterized by resonances unstable under the strong interaction whose properties are encapsulated within momentum-dependent phase shifts. In lattice calculations, shifts in the energy spectrum at finite volume can be related to infinite-volume phase shifts[50, 119]; recently, the energy-dependent phase shift of the ρ resonance in $\pi\pi$ elastic scattering has been mapped in unprecedented detail[120].

The next five years present an exciting opportunity for lattice QCD to work in concert with experiment to *predict* the underlying features of spectrum in advance of experiment. With the first experiments at the 12GeV upgrade of Jefferson Laboratory expected in 2015, a proposed detector PANDA at the FAIR facility in Germany, and an on-going program at COMPASS at CERN, a vibrant program will compute:

- *The spectrum of the low-lying meson resonances*

  Computations at the physical quark masses will enable the spectrum of hybrid mesons to be confidently calculated, and the confrontation of the QCD calculations with experimental extractions of states in the region of sensitivity of GlueX of 1.8 to 2.7 GeV, thus capitalizing on the **2018 NSAC Performance Measure HP15**. Paramount will be a theoretical effort at developing methods of treating coupled-channel effects and multi-hadron states that appear above the inelastic threshold[56, 121–125], the focus of a recent program at the *Institute for Nuclear Theory*.

- *The spectrum of excited baryon resonances* The excited-state spectrum of all the excited baryons that can be constructed from the u, d and s quarks will elucidate the role of quark flavor and mass in the spectrum of QCD. For the Ξ and Ω in particular, our experimental knowledge and the production of such "very strange" baryons is proposed with both the CLAS12 and GlueX detectors at the 12 GeV upgrade of JLab.

Precise calculations of the N^* spectrum at the physical pion masses will fully capitalize on the experimental baryon resonance program and the achievement of the **2009 NSAC Performance Measure HP3**. Finally, a knowledge of the decay modes and widths of excited states can address key questions that might guide experiment, such as whether the doubly strange Cascades are really narrower than baryons composed of the light quarks.

- *Electromagnetic properties of Excited States*

  The *GlueX* experiment aims to photoproduce excited mesons whereby photons are anticipated as a means of preferentially producing hybrid states. Calculations of the photocouplings to excited mesons will inform the expected photoproduction rates in experiment, and provide clues as to their internal structure. In the baryon sector, calculations of the $\gamma NN*$ electrocouplings at $Q^2 < 5$ GeV^2 will elucidate the role of pionic degrees of freedom, whilst calculations at high Q^2 will explore the transition from the large-distance scales with confinement-dominated dynamics, to the short-distance scales with perturbative-dominated dynamics.

Recent advances in understanding the excited-state spectrum of QCD have exploited so-called anisotropic Wilson clover lattices, which have a fine temporal lattice spacing of $a_r = 0.035$ fm to enable the resolution of many levels in the spectrum, but a coarser spatial lattice spacing of $a = 0.12$ fm. The availability of isotropic Wilson clover lattices at spacings of $a = 0.09$ fm and below is anticipated to render the use of an anisotropic lattice redundant. Our five-year program therefore anticipates a comparison of the spectrum between the two actions at pion mass of 200 MeV as a validation before undertaking the above program at the physical quark masses on an isotropic Wilson clover lattice. The cost of our program is laid out in the Table IV, denoted by "HSp". Should resources beyond Moore's law projections become available, they will facilitate calculations at a finer lattice spacing and at larger volumes, thus constraining discretization uncertainties.

3. Hadronic Interactions, Nuclear Forces, Nuclei and Hypernuclei

As the standard model of elementary particles is responsible for the nuclei and their interactions, lattice QCD promises to provide a rigorous underpinning for nuclear physics. We anticipate that nuclear interactions will be systematically refined by lattice-QCD calculations, and the uncertainties associated with future predictions of nuclear processes will be fully quantified. Equally important, lattice QCD allows for the quark-mass dependence of nuclear structure and the nuclear forces to be precisely determined, providing a detailed exploration of fine-tunings that define our universe. Serious efforts to determine the properties and interactions of the light nuclei, leading to nuclear forces which can be propagated throughout the periodic table, have been underway for nearly a decade by the NPLQCD collaboration [126–131] and also by two Japanese collaborations [132–135]. These calculations have been performed with the clover action at one lattice spacing in the isospin limit and without electromagnetism by three lattice collaborations. The deuteron binding energy has been determined at pion masses of $m_\pi \sim 400, 500$ and 800 MeV [126, 127, 130, 132–135], with as yet insufficient precision. Similar calculations have shown the di-neutron to be bound at these heavier pion masses, and all of the presently accessible two-baryon octet

channels contain a bound state at the SU(3) symmetry point. The deepest bound state at the heavier pion masses is the H-dibaryon [128, 129, 136], as conjectured in the 1970's. After significant developments in algorithms to efficiently evaluate Wick contractions [137], correlation functions for systems $2 < A < 6$ can now be constructed, and have lead to the first comprehensive study of s-shell nuclei and hypernuclei [129–131] (*albeit* at unphysical light-quark masses), along with nucleon-nucleon scattering parameters. The nucleon-nucleon phase-shifts, scattering lengths and effective ranges in both spin-channels have been determined at the SU(3) symmetric point. The interactions between hyperons and nucleons is a crucial element in dictating the behavior and composition of dense matter, such as that which may be created in core-collapse supernovae. The first predictions for such interactions, extrapolated to the physical light-quark masses has been made during the last year, and future calculations will refine such predictions beyond what is possible experimentally at this time. A detailed understanding of the interactions between mesons, and between mesons and baryons, is crucial to the success of the experimental baryon resonance and exotic meson program that will be performed with the 12 GeV upgrade at JLab. These types of processes are being explored simultaneously with the nuclear interactions program. This program is the rationale that underpins the **2014 NSAC Performance Measure HP10**.

For the next five years, the key research drivers in this area of research are: a) *Nucleon-Nucleon Interactions and the Deuteron*, b)*Hyperon-Nucleon Interactions and the Core of Neutron Stars*, c)*S-Shell Nuclei and Hypernuclei, and their Interactions*, and d)*P-Shell Nuclei and Hypernuclei*. If resources available to this area of research increase with Moore's law, calculations of s-shell and p-shell nuclei will be performed at pion masses of $m_\pi \sim 250$ MeV, $m_\pi \sim 200$ MeV, and $m_\pi \sim 140$ MeV using the isotropic clover discretization, as shown in the column labeled "HI" in Table IV, and will provide the first post-dictions of light nuclei at the physical pion mass. Except for the deuteron, which is unnaturally large, the binding of the light nuclei is not expected to depend sensitively upon the light-quark masses, and as such, these calculations will provide for a quantification of the systematic uncertainties introduced by the lattice discretization. Therefore, the chiral nuclear forces will be determined from QCD, including the multi-neutron interactions that are presently poorly constrained by experiment but will be refined by FRIB. One subtle feature is that calculations away from the physical light-quark masses are essential for fully dissecting the chiral nuclear forces and refining the existing interaction phenomenology. The proposed calculations are expected to be sufficient to accomplish an approximate decomposition of these forces, and will allow for predictions of other elements of the periodic table of elements at the physical pion mass through matching to existing and developing nuclear many-body calculations through collaboration with the broader nuclear physics community. If the available resources were to scale faster than Moore's law, and if developments in algorithms continue at the present rate, we expect to perform calculations of nuclei at the physical point with multiple lattice spacings and volumes.

4. Fundamental Symmetries

Research efforts to uncover particles and symmetries beyond those of the standard model of the strong and electroweak interactions are multi-pronged. There is an ongoing experimental program focused on the magnetic moment of the muon. The E821 experiment at Brookhaven National Laboratory has measured the muon $g-2$ with an uncertainty of 0.7 ppm, which

deviates from the theoretical calculation by $\gtrsim 3\sigma$. The approved E-989 experiment at Fermilab is designed to reduce the uncertainty in $g-2$ below 0.14 ppm, either verifying the discrepancy with theory or resolving it. A major uncertainty in the theoretical calculation arises from strong interactions through quantum loops. Exploratory lattice-QCD calculations of the muon $g-2$ are underway to understand how to calculate the strong interaction contributions[64, 66, 138], discussed also in Sec. II A 2.

The nEDM collaboration is preparing to measure the electric dipole moment (edm) of the neutron a quantity that vanishes in the absence of time-reversal, T, violation (equivalent to CP-violation when CPT-invariance is exact), with a precision of $\delta d_n \sim 3 \times 10^{-28}$ e cm at the Spallation Neutron Source (SNS) at Oak Ridge National Laboratory. There have been a number of efforts, part of the broader effort to support the **2020 NSAC Performance Measure FI15**, to calculate the neutron edm arising from the QCD θ-term using lattice QCD [139, 140]. During 2010, the first lattice QCD calculation of nuclear parity violation was performed at a pion mass of $m_\pi \sim 390$ MeV [141], in which the connected diagrams contributing to the weak one-pion-nucleon vertex, $h^1_{\pi NN}$, were determined. Its value at unphysically large light-quark masses was found to be consistent with the unnaturally small value extracted from theoretical analyses of a number of experimental measurements. An ongoing experimental effort by the NPDGamma Collaboration [142] at the SNS promises to greatly reduce the experimental uncertainties in the value of $h^1_{\pi NN}$, likely in a similar timeframe to the lattice-QCD calculations. In anticipation of precise experimental constraints on the structure of the four-Fermi operators contributing to the β-decay of ultra-cold neutrons, lattice-QCD calculations are underway to determine the strong interaction contributions to the matrix elements of such operators. Observation of a transition of neutrons to antineutrons could provide distinct evidence for baryon number violation from beyond the standard model physics. GUTs predict oscillation periods of between 10^9 and 10^{11} seconds. Matrix elements of the relevant operators will be evaluated with lattice QCD, eliminating uncertainty from the oscillation period estimates and sensitivity of current and future experiments.

The main research thrusts during the next five years are: *Electric Dipole Moments of the Neutron, Proton and Deuteron*, *Strong Interaction Contributions to the Muon Magnetic Moment*, *Nuclear Parity Violation*, and *Physics Beyond the standard model in Four-Fermi Operators*. We anticipate that the resource requirements required for these calculations can be accommodated by those provided to the Hadron Structure, Hadron Spectrum and Hadronic Interactions research directions.

5. Resource Requirements

The computational requirements to perform the physics program detailed above is provided in Table IV. The cost is amortized across different parts of our program by the use of gauge configurations for a variety of nuclear-physics and intensity-frontier problems. Should computational power proceed faster than Moore's law, and algorithms advance at their present rate, the still more ambitious program of computations referenced above would be feasible.

C. Computational Challenges in QCD Thermodynamics

To a large extent complex many-body interactions control the various phases of strong interaction matter,which are relevant to our understanding of the nuclear force and its role

TABLE IV: Resources for the program of calculations in Sec. II B. We show the lattice sizes, fermion actions, labeled as isotropic Wilson-clover (W), anisotropic Wilson-clover (AW) and domain-wall (DWF), and the cost of generating the configurations; those for DWF listed in Table II are not repeated. Entries in the last four columns show the cost of the measurement calculations proposed on each of the ensembles: two for hadron structure (Str-A and Str-B), one for hadron spectroscopy (HSp) and one for hadronic interactions (HI). For the Str-B measurements, the additional cost of high-precision isovector calculations and the disconnected contributions to flavor-separated quantities are denoted by † and ∗ respectively.

$N_s^3 \times N_t$	Action	a	m_π	$m_\pi L$	$m_\pi T$	Traj.	Configs.	Str-A	Str-B	HSp	HI
		fm	MeV				(TF-yrs)		(TF-yrs)		
$64^3 \times 128$	W	0.076	250	6.1	12.3	5×10^3	8				
$64^3 \times 128$	W	0.09	200	5.8	11.7	5×10^3	9			167	27
$32^3 \times 512$	AW	0.12	200	3.8	17.6	1×10^4	44			41	
$48^3 \times 512$	AW	0.12	200	5.8	17.6	1×10^4	197			142	
$48^3 \times 192$	W	0.09	140	3.0	12.3	5×10^3	7	40			
$64^3 \times 192$	W	0.09	140	4.1	12.3	5×10^3	21	40			
$96^3 \times 64$	W	0.09	140	6.1	4.1	5×10^3	24	13			
$96^3 \times 96$	W	0.09	140	6.1	6.1	5×10^3	40	20			
$96^3 \times 192$	W	0.076	140	6.1	12.3	5×10^3	96	40	350*	334	288
$128^3 \times 192$	W	0.076	140	6.9	10.4	5×10^3	323	67		792	970
$48^3 \times 96$	DWF	0.110	140	3.9	7.8	5×10^3		28	360†		
$64^3 \times 128$	DWF	0.086	140	3.9	7.8	5×10^3		64	844†		
Total structure, spectrum, and interactions of hadrons resource estimate											5,396

in determining the structure of nuclear matter. Accounting for their effects quantitatively requires nonperturbative techniques, such as the numerical simulation of QCD. Such simulations are of particular importance in the temperature range close to phase changes, where properties of the matter change rapidly. This temperature range is currently also probed experimentally in relativistic heavy-ion experiments.

During the next years we will see a large number of new experimental results from heavy ion experiments at RHIC as well as the Large Hadron Collider at CERN. The latter will probe the high temperature phase of QCD at almost vanishing net baryon number in a wider temperature range, providing new information about thermal dilepton and photon emission from the quark-gluon plasma, heavy quark bound states, the equilibration and diffusion of light and heavy quarks in dense matter, as well as information about other transport coefficients that characterize the *perfect fluid* [143–147]. Furthermore, the Beam Energy Scan (BES) [148, 149], recently performed at RHIC, and, we hope, to be continued in upcoming years, will provide much information about fluctuations in net proton and net electric charge numbers, which will allow us to explore the phase diagram at nonzero baryon chemical potential (μ_B); detector upgrades of STAR and PHENIX will lead to new high precision data on properties of strong interaction matter close to the QCD transition. Providing theoretical input from lattice QCD

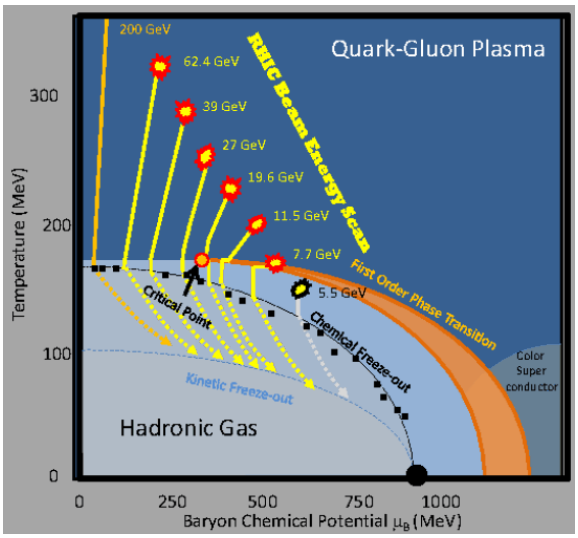

FIG. 3. Schematic phase diagram of OCD, including a still hypothetical critical point, and the parameter range covered by the current beam energy scan at RHIC [148].

calculations at vanishing as well as nonvanishing values of μ_B, extrapolated to the continuum limit and performed with physical quark mass values, thus remains of great importance.

Aside from these experiment-driven motivations for future numerical calculations in QCD thermodynamics, there also exist fundamental theoretical questions related to the phase structure of QCD at nonzero temperature and density that should be addressed, as QCD is the only component of the standard model that stands on its own as a well-defined quantum field theory. The spontaneously broken chiral symmetry, the axial anomaly and the topological structure of the QCD vacuum have played an important role in the development of our theoretical picture of the QCD phase diagram. Clarifying the role and interplay of these nonperturbative mechanisms also is of importance for the development of possible beyond-the-standard-model theories.

With the increase in computing resources, we have now reached a point at which numerical simulations not only with physical values of quark masses but even with mass parameters smaller than physical have become possible. This will allow us to come close to the chiral limit of QCD and directly probe the universal properties of QCD thermodynamics, including the existence of genuine phase transitions at $\mu_B \geq 0$ which is searched for in the BES at RHIC and is a central motivation for new research facilities such as FAIR in Germany and NICA in Russia.

1. The QCD transition at vanishing and non-vanishing baryon number density

The QCD transition temperature and the equation of state are among the most basic quantities of QCD thermodynamics that are of obvious importance for the description of the hydrodynamic expansion of hot and dense matter created in heavy ion experiments as well as the early universe. One of the highlights of research in this field is the consensus reached in recent years on the QCD transition temperature at $\mu_B = 0$ and the variation of this transition temperature with μ_B. An analysis of the pseudo-critical temperature at the crossover transition using three different staggered fermion actions (P4, asqtad and HISQ) extrapolated to the continuum limit gave the value $T_c = 154(9)$ MeV [150]. This value is in good agreement with results obtained by using the stout staggered fermion action [28] and it is also close to experimentally determined freeze-out temperatures in high energy runs at RHIC [151]. Furthermore, for $\mu_B > 0$ the experimentally determined freeze-out temperatures seem to agree well with the temperature for the QCD crossover transition in a wide range of baryon chemical potentials, $\mu_B \lesssim 200$ MeV, which corresponds to beam energies at RHIC of $\sqrt{s_{NN}} \gtrsim 20$ GeV (see Fig. 4). The lattice-QCD calculations of the transition temperature at $\mu_B > 0$ are based on next-to-leading order Taylor expansions of thermodynamic observables.

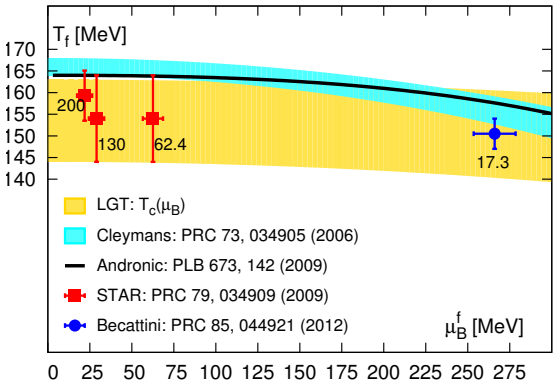

FIG. 4. The QCD transition compared with freeze-out temperatures determined at RHIC and the SPS. The broad band shows the transition temperature $T_c(\mu_B) = T_c(0) + \kappa_B(\mu_B/T)^2$ with $T_c(0) = 154(9)$ MeV [150] and $\kappa_B = 0.0066(7)$ [152] obtained in lattice-QCD calculations.

Extending and improving these studies of the phase diagram at nonzero baryon number and the comparison with experimental findings [153] will be the central topic of next generation lattice calculations. This requires (i) to increase the predictive power of Taylor expansions at $\mu_B > 0$ by going to higher orders in the expansion and reducing the statistical errors on results for the expansion coefficients; and (ii) to firmly establish the universal scaling properties of the chiral transition at zero and nonzero chemical potential by performing calculations with lighter-than-physical quark masses and using lattice discretization schemes with exact chiral symmetries for studies of the QCD transition.

2. Taylor expansions and the QCD critical endpoint

It has been postulated that at large values of μ_B a second order phase transition point shows up which is the endpoint of a first order phase transition line. Whether or not a true second order phase transition point, the critical endpoint [154], exists in the QCD phase diagram for $\mu_B > 0$ is one of the most exciting questions in current studies of QCD thermodynamics. The beam energy scan program at RHIC is devoted to this question. Much of this experimental program is motivated by lattice-QCD studies that showed the sensitivity of fluctuations of conserved charges and their higher order cumulants to changes in temperature and baryon chemical potential [157, 158]. In particular, ratios of higher order cumulants of conserved charge fluctuations are interesting as they directly reflect the most relevant degrees of freedom that are carriers of these charges in different temperature regimes [155, 156] (see Fig. 5) and, moreover, are also accessible in heavy ion experiments [159]. The BES at RHIC produced first results on fluctuations of net proton numbers and net electric charge [160–162] that now can be compared with lattice QCD calculations [153, 163]. In Fig. 3 we show a schematic plot of the QCD phase diagram including a critical point and the parameter range of the BES at RHIC that is currently pursued in search for hints for its existence and location. In order to address this issue in lattice-QCD calculations based on a systematic expansion in μ_B one has to calculate accurately higher order expansion coefficients in Taylor series of, *e.g.*, the baryon number susceptibility. An accurate calculations of ratios of cumulants χ^B_{n+2}/χ^B_n is needed at temperatures $T \lesssim 160$ MeV in order to construct estimators for the radius of

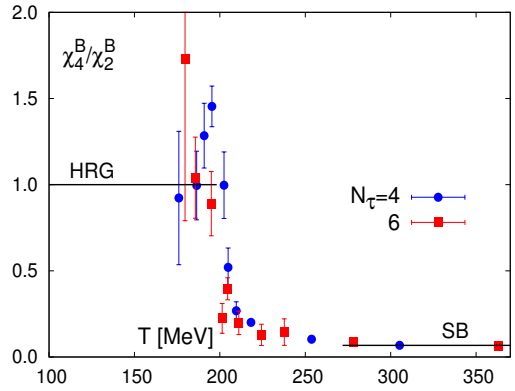

FIG. 5. The ratio of quartic and quadratic fluctuations of net baryon number. The rapid change in this ratio shows that baryon number is carried by hadrons ($B^2 = 1$) at low temperatures and quarks ($B^2 = 1/9$) at high temperature [155, 156].

convergence of Taylor series, that may also provide hints for the existence of such a critical point.

Calculations of higher order cumulants typically require generation of $O(10^5)$ gauge-field configurations. On a sub-sample of $\mathcal{O}(10^4)$ configurations, susceptibilities are calculated through multiple inversions of the fermion Dirac matrix using $\mathcal{O}(10^3)$ random source vectors. The calculation of higher order cumulants at a single value of the temperature thus typically involves several million matrix inversions. The number of random vectors plus gauge-field configurations needed to reach comparable statistical errors in n^{th} order cumulants grows exponentially ($\sim \exp(2n)$) . The overall computational effort for adding another nonzero expansion coefficient in the Taylor series thus increases roughly by two orders of magnitude.

Such calculations will need substantial computing resources for the generation of gauge-field configurations and the calculation of Taylor expansion coefficients. In particular the latter is done efficiently on general purpose graphics processing units (GPUs). State-of-the-art calculations of cumulants continuously make use of $\mathcal{O}(500)$ GPUs. In order to advance to the calculation of eighth order cumulants one will need to exploit computing platforms with several thousand GPUs or next generation multi-core processors like Intel's MIC.

3. Universal properties of the chiral transition and its impact on the real world

During recent years calculations at and below the physical quark mass values have become possible with improved staggered fermion actions. For the first time this has allowed a convincing demonstration of the existence of an underlying universal structure in thermodynamic functions that is consistent with the scaling properties expected for a phase transition in the three-dimensional $O(4)$ universality class [164] (see Fig. 6). Still these findings are not unchallenged. The possibility for having a first order phase transition in the chiral limit of 2-flavor QCD is still being advocated [165]. Clearly this fundamental theoretical questions, which also impacts our thinking about the phase diagram at nonzero baryon chemical potential, needs to be addressed. In order to reach firm results on the order of the transition in the chiral limit, the studies of universal properties need to be performed closer to the continuum limit and with smaller-than-physical quark masses. Moreover, calculations with chiral fermions will be needed to address also subtle issues related to the axial anomaly.

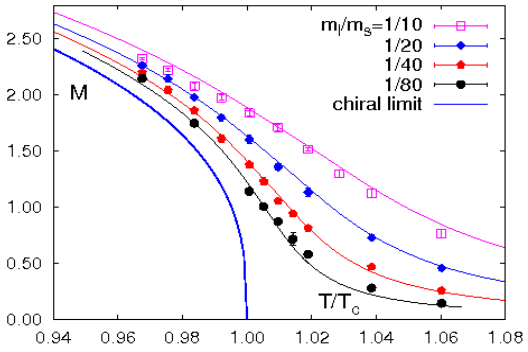

FIG. 6. Scaling behavior of the normalized chiral condensate, $M = m_s\langle\bar{\psi}\psi\rangle/T^4$, for different values of the light-to-strange quark mass ratio m_l/m_s on coarse lattices with temporal extent $N_\tau = 4$ [164].

As noted already in the seminal work on the phase structure of QCD in the chiral limit [166], the axial anomaly plays a crucial in role in defining the qualitative aspects of the phase structure of dense QCD, specially on the existence/location of the QCD chiral critical point [167]. To address these intriguing phenomenological as well as theoretical issues via nonperturbative lattice QCD, it is obviously preferable to utilize a discretization scheme, such as domain wall fermions, that preserves exact chiral symmetry and reproduces the correct axial anomaly even at nonvanishing values of the lattice spacing. First results obtained

with DWF on the QCD transition [168] and axial symmetry breaking at finite temperature [169] are indeed encouraging. These exploratory studies indicate that the relation between low-lying eigenvalues of the Dirac operator, enforced by the exact chiral symmetry of DWF, and the topological structure of gauge-field configurations becomes evident. In the future these DWF studies need to be extended toward the chiral limit by utilizing smaller quark masses for detailed explorations of the chiral symmetries in QCD.

4. The properties of the quark-gluon plasma

Experiments at RHIC have revealed that even at temperatures moderately above the QCD transition temperature, the quark-gluon plasma exhibits far more complex properties than that expected for a weakly interacting thermal medium described by perturbative QCD [143–147]. In particular, the QGP possesses remnant confining features, *i.e.*, some hadronic bound states involving heavy quarks continue to exist in this regime. Furthermore, these highly non-perturbative properties of the QGP also results in intriguing transport properties leading to many unexpected experimental observations: the smallness of the ratio of shear viscosity and entropy density leads to (almost) perfect fluidity of the QGP. Understanding the properties of this genuinely nonperturbative regime in the high temperature phase of QCD is a theoretical challenge that requires a genuine to the continuum limit using physical values of the dynamical quark masses.

Heavy quark spectroscopy: Lattice calculations of heavy quark bound states have advanced considerably in recent years. Finite temperature calculations in quenched QCD are now possible on lattices as large as $128^3 \times 96$ [170], which is comparable to lattice sizes used in zero temperature hadron spectroscopy. Such large lattices with a high resolution allow us to study the thermal heavy quark correlation function and provide enough information on the Euclidean time dependence of these correlators to perform a statistical analysis based on the maximum entropy method (MEM) [171]. This allows to calculate spectral functions as well as transport coefficients. Some recent results for the J/ψ spectral function are shown in Fig. 7. They lead to the conclusion that all charmonium states have melted at $1.5T_c$. First attempts to generalize these calculations to properties of bound states at nonzero momenta [172] are underway, and also first attempts to study heavy quark bound states, including the bottomonium system, in QCD with a dynamical light quark sector have been started [173]. The latter, however, are at present limited to studies on rather small lattices and a major computational effort is needed to perform these calculations on lattices as large as $128^3 \times 96$.

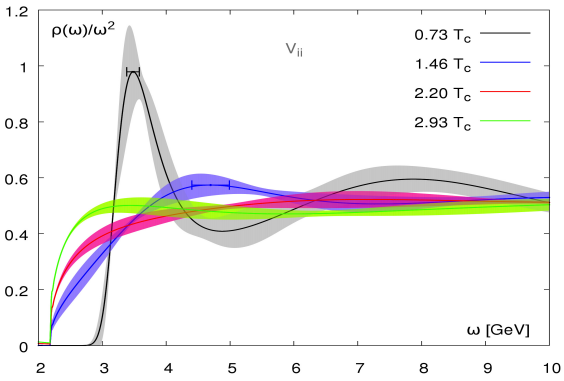

FIG. 7. The spectral function of the charmonium ground state at different values of the temperature [170] calculated in quenched QCD.

Thermal gauge-field configurations on lattices with large temporal extent also permit an analysis of spectral functions in the light quark sector. Aside from showing explicitly that light quark bound states in different quantum number channels melt in the high temperature

phase, the vector spectral function is of particular interest. It provides direct information about the production rate for dilepton pairs arising from quark anti-quark annihilation in a hot thermal medium. Recent calculations on large quenched QCD lattices of sizes up to $128^3 \times 48$ [174] yield continuum extrapolated results that are in good agreement with resummed perturbation theory. An extension of these calculations to nonzero momentum is underway and will also give access to thermal photon rates. Of course, in the light quark sector it will be even more important than for heavy quarks to include contributions from dynamical light quarks in these calculations.

Transport and diffusion coefficients: A problem closely related to the analysis of light and heavy quark bound state properties is the calculation of light and heavy quark transport properties, *e.g.*, the electrical conductivity and the heavy quark diffusion constant. This requires gaining control over the low frequency region of spectral functions, which is even more sensitive to the large distance behavior of correlation functions and thus requires large lattices and good control over statistical errors. Usually, one needs an ansatz for the functional form of the spectral function in this regime, e.g., $\rho(\omega) \sim \omega$, to extract transport coefficients. First results on the electrical conductivity [174] and the heavy quark diffusion constant [170] have been obtained in connection with the recent studies of light and heavy quark correlation functions on large quenched lattices (see Fig. 8). Extending these calculations to QCD with dynamical light quark degrees of freedom on similar size lattices will be an important task during the next years. The largest influence of dynamical quark degrees of freedom will become visible in the transition region. A calculation of spectral functions thus can focus on a few temperature values in the range $T/T_c \simeq (1 - 1.5)$. Large lattices ranging from $128^3 \times 32$ to $256^3 \times 64$ will be needed to control the extrapolation to the continuum limit. Calculations of shear and bulk viscosities follow a similar strategy. However, their analysis involves the noisy gluonic part of the energy momentum tensor. Such calculations thus require about an order of magnitude more resources and will be possible only on smaller lattices.

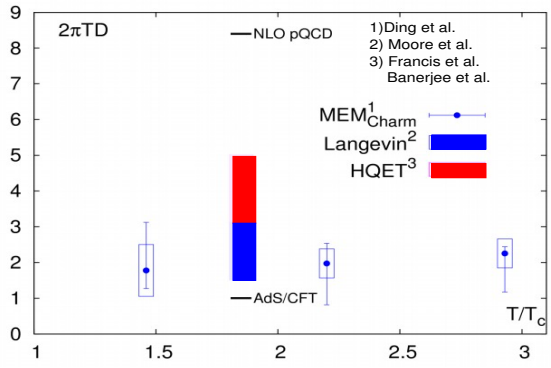

FIG. 8. Heavy quark diffusion constant (D) calculated in quenched lattice QCD (MEM) [170]. Results are compared to perturbative (NLO pQCD), AdS/CFT calculations, Langevin modeling of the diffusion process and heavy quark effective theory.

Project	lattice size	temps	quark masses	trajecs per param. set	cost [TFlo/ps-years]
phase boundary at $\mu > 0$ in the chiral limit	$(6A)^3 \times 6$ $6 \leq A \leq 12$	5	3	100,000	750
higher order cumulants of conserved charges	$(4N_\tau)^3 \times N_\tau$ $N_\tau = 8,\ 12,\ 16$	4	1	100,000	2,900
light and heavy quark spectral functions	$(4N_\tau)^3 \times N_\tau$ $N_\tau = 32,\ 48$	3	1	10,000	450
	$N_\tau = 64$	3	1	5,000	500
bulk and shear viscosities	$(3N_\tau)^3 \times N_\tau$ $N_\tau = 32,\ 48$	1	1	50,000	800
chiral transition with chiral fermions	$(8A)^3 \times 8$ $A = 6,\ 8$	5	2	10,000	500
Total QCD thermodynamics resource estimate					5,900

Table V: Summary of simulation parameters and cost estimates for QCD thermodynamics. Cost estimates are based on current experience with calculations on leadership class computers (BlueGene/Q) and GPU enhanced clusters.

5. Computational Requirements

All of the ongoing and future research projects outlined above are in need of large computational resources that cannot be expected to be fully realized during the next years. In our studies of transport coefficients we thus will perform complete calculations for two different lattice sizes and plan to start studies on an additional larger lattice with reduced statistics, which will be increased once additional resources become available. A pilot study of the bulk and shear viscosities will need to be restricted to a single temperature value. Studies of the chiral transition with DWF will be performed with two different light quark masses and calculations for a third, lighter quark mass will be added at a later stage.

D. Strongly Coupled BSM Gauge Theories at the Energy Frontier

The recent discovery of the Higgs-like resonance at 126 GeV by the CMS [175] and ATLAS [176] experiments at the Large Hadron Collider (LHC) provides a watershed insight into the origin of electroweak symmetry breaking (EWSB). The standard model realization of EWSB is implemented by introducing an elementary SU(2) doublet scalar Higgs field whose vacuum expectation value sets the electroweak scale. This simple solution is generally regarded to be a phenomenological parametrization rather than a full explanation of EWSB. In particular, the mass-squared parameter of the light Higgs has to be finely tuned, leading to the well-known hierarchy problem. Searching for a deeper dynamical explanation, and resolving the shortcomings of the elementary standard-model Higgs, the USQCD BSM program has developed three major research directions. One direction employs strongly coupled gauge theories near conformality [177–181], another direction envisions the new particle

as a light pseudo-Goldstone boson (PNGB) in the spirit of little Higgs scenarios [182–189], and the third direction begins to explore the non-perturbative dynamics of SUSY gauge theories. In each of these three research directions, new degrees of freedom are expected at the TeV scale with important implications for the LHC experimental program at the Energy Frontier.

In the past few year USQCD lattice-BSM research has begun to demonstrate the potential of lattice field theory to investigate non-perturbative consequence of these BSM conjectures:

- Investigations of strongly coupled BSM gauge theories identified conformal or near conformal behavior, demonstrating that the anomalous mass dimensions and chiral condensates are enhanced near conformality, with interesting implications for model building.
- Electroweak precision experimental constraints were compared with numerical estimates of the S-parameter, $W - W$ scattering, and the composite spectra. In particular in contrast with naive estimates, these studies demonstrate that the S-parameter in near-conformal theories may be reduced in better agreement with experimental constraints.
- Investigations of $\mathcal{N} = 1$ supersymmetric Yang Mills theory (gauge bosons and gauginos) produced estimates of the gluino condensate and string tension in these theories.

Building on these significant and computationally demanding accomplishments, challenges and prospects are identified in all three major research directions of the USQCD BSM program with emphasis on the broad range of phenomenological applications and the development of new lattice-field-theory methods targeted at BSM physics.

1. The light Higgs and the dilaton near conformality

In the absence of electroweak symmetry breaking, the interactions of standard-model gauge bosons and fermions show approximate conformal symmetry down to the QCD scale. This opens up the possibility that the Higgs mode and the dilaton mode, the pseudo-Goldstone boson of spontaneously broken scale invariance, are perhaps intimately related. The important properties of the standard-model Higgs boson are basically determined by the approximate conformal invariance in the limit when the Higgs potential is turned off. In this case the Higgs vacuum expectation value (vev) is arbitrary (it is a flat direction), and its value at $v = 246$ GeV will spontaneously break the approximate conformal symmetry and the electroweak symmetry. In this limit the Higgs particle can be identified with the massless dilaton of conformal symmetry breaking [181]. Higgs properties in this weak coupling scenario are associated with approximate conformal invariance.

If the strongly coupled BSM gauge model is very close to the conformal window with a small but nonvanishing β-function, a necessary condition is satisfied for spontaneous breaking of scale invariance and generating the light PNGB dilaton state. For any choice of the fermion representation R of the color gauge group, the conformal window is defined by the range of the flavor number N_f for which the β-function has an infrared fixed point, where the theory

is in fact conformal. Since near-conformal models exhibit chiral symmetry breaking (χSB) a Goldstone pion spectrum is generated and when coupled to the electroweak sector, the onset of electroweak symmetry breaking with the Higgs mechanism is realized. This might create a natural setting with minimal tuning for a light Higgs-like particle [190]. Although this scalar state has to be light it would not be required to exhibit exactly the observed 126 GeV mass. The dynamical Higgs mass $M_H^{0^{++}}$ from composite strong dynamics is expected to be shifted by electroweak loop corrections, most likely dominated by the large negative mass shift from the top quark loop [191].

The very small beta function (walking) and χSB are not sufficient to guarantee a light dilaton state if scale symmetry breaking and χSB are entangled in a complicated way. However, a light Higgs-like scalar might still be expected to emerge near the conformal window as a composite scalar state with 0^{++} quantum numbers. Close to the conformal edge, the generic features and the required resources for the scalar spectrum have been investigated in pilot studies of frequently discussed BSM gauge theories with eight and twelve fermion flavors in the fundamental representation of the SU(3) color gauge group [192, 193], and the sextet model with a fermion doublet in the two-index symmetric (sextet) representation of the SU(3) color gauge group [194, 195]. Although the precise position of these models with respect to the conformal window is not resolved, the required lattice technology to capture the scalar spectrum in BSM lattice models is quite robust in a model independent way.

In BSM models, close to the conformal window, a low mass 0^{++} glueball is expected to mix with the composite scalar state of the fermion-antifermion pair. With the ultimate goal of reaching to the chiral limit of massless fermions, the mixing scheme in the scalar spectrum has to also include Goldstone pairs with vacuum quantum numbers and exotic states made of two fermions and two antifermions with 0^{++} quantum numbers. Realistic studies require a 3-channel solution, even if exotica are excluded from the analysis. The pilot studies for planning of this proposal were restricted to the single channel problem using scalar correlators which are built from connected and disconnected loops of fermion propagators.

In addition to studies of the scalar spectra, plans for studies of near-conformal gauge theories include the calculation of the chiral condensate and its spectral representation, the S-parameter, WW-scattering, the running coupling, and predictions of dark matter from compositeness.

2. Higgs as a pseudo-Goldstone boson

With the discovery of a new particle at 126 GeV with properties so-far consistent with the standard model Higgs boson, it is natural to explore strong dynamics where this Higgs is a scalar pseudo-Nambu-Goldstone boson (PNGB). This PNGB Higgs mechanism [196] plays a crucial role in little Higgs [197, 198] and minimal conformal technicolor [199] models. In little Higgs theory, an interplay of global symmetries is devised in an effective Lagrangian to cancel the quadratic divergences for the Higgs mass to one loop. This provides a weakly coupled effective theory with little fine tuning up to energies on order of 10 TeV. A large range of phenomenologically interesting models continues to be explored as weakly coupled extensions of the standard model with PNGB Higgs scalars.

Lattice field theory can explore fully non-perturbative realizations of this approach, starting with an ultraviolet complete theory for strongly interacting gauge theories with fermions in

real or pseudo-real representations of the gauge group giving rise to Goldstone scalars. In the chiral limit the Higgs scalar is a member of set of Goldstone Bosons that includes the triplet of "techni-pions", required to give masses to the W and Z. Consequently, the mass of this Higgs is naturally light with its mass induced by small couplings to the weak sector. A central challenge to support this scenario for models based on effective phenomenological Lagrangian is to use lattice field theory to demonstrate that viable UV complete theories exist and to understand the impact of extending the standard model with this strong sector replacing the weakly coupled elementary Higgs.

Simulation of the Minimal PNGB Model

Our first goal is to study a minimal realization of the PNBG for the Higgs and to demonstrate the predictive power of *ab initio* lattice solutions of the strong sector. The minimal PNBG Higgs model consists of a $SU(2)$ color gauge theory with $N_f = 2$ fundamental massless fermions. Additional sterile flavors with $N_f > 2$ can be added [199] to drive the theory close to or into the conformal window. Because of the pseudo-real properties of $SU(2)$ color group, the conventional $SU(N_f)_L \times SU(N_f)_R$ vector-axial symmetry becomes a larger $SU(2N_f)$ flavor symmetry combining the $2N_f$ left/right 2-component chiral spinors. Most-attractive-channel arguments, confirmed by lattice simulations, imply that $SU(2N_f)$ will break dynamically to $Sp(2N_f)$. If explicit masses are given to $N_f - 2$ flavors, the remaining 2 massless flavors yield the $SU(4)/Sp(4)$ coset with 5 Goldstone Bosons: the isotriplet pseudo-scalars (or "techni-pions") to give mass to the W, Z, and two isosinglet scalars. The top quark provides an additional explicit breaking, so that these two extra Goldstone Bosons become massive. The lighter is a candidate for a composite Higgs and the heavier is a possible candidate for dark matter.

A important consideration is the choice of action: staggered, Wilson or domain wall? Our first choice is to start with the Wilson action while we investigate further possible advantages for the least expensive staggered case and more expensive domain wall case. The Wilson term breaks chiral symmetry but fortunately it aligns the vacuum consistent with the breaking of $SU(4)$ to $Sp(4)$. Research is underway to see if domain wall fermions at finite lattice spacing have, as expected, the full enhanced $SU(4)$ symmetry at infinite wall separation. If this is proven to hold, clearly the domain wall implementation, although more costly, does have theoretical advantages worth considering. Most likely, as has proven to be the case in lattice-QCD research, each action will prove to be advantageous for specific questions.

3. Studies of supersymmetric theories on the lattice

Supersymmetric theories have been extensively studied over many decades now both as providing natural models for electroweak symmetry breaking and in the context of string theory. However, for many years, significant barriers prevented serious nonperturbative study of such theories on the lattice. Recently this has changed; new theoretical formulations and improved algorithms and hardware have enabled pioneering studies to be made of a number of supersymmetric theories including both $\mathcal{N} = 1$ and $\mathcal{N} = 4$ super Yang-Mills. $\mathcal{N} = 1$ super Yang Mills is the supersymmetric analog of pure QCD and as such is the first step on the road to understanding the structure of super QCD.

Understanding super QCD is important because most of the low scale supersymmetric BSM models currently on the market contain explicit supersymmetry breaking soft parameters

which are needed since the low energy world is manifestly not supersymmetric. While currently the values of these soft parameters are typically obtained from fits to experimental data it is believed that in general they are determined by non-perturbative supersymmetry breaking in some high scale *hidden sector* theory. Super QCD can play the role of such a hidden sector theory.

Dynamical SUSY breaking and super QCD

In generic so-called gauge mediation models the hidden sector fields must be coupled to the fields in any low scale BSM sector so that when supersymmetry is broken in the hidden sector it is communicated to the BSM fields via a small number of non-perturbatively determined vacuum expectation values. For a strongly coupled hidden sector these vevs can be computed using lattice simulation.

There are powerful theoretical arguments that N_c-color super QCD with N_f number of flavors of fermion possesses long lived metastable SUSY breaking vacua [200] if $N_c + 1 \leq N_f < \frac{3}{2}N_c$. Within such a vacuum state non-perturbative phenomena such as confinement and chiral symmetry breaking precipitate such a breaking of supersymmetry. Furthermore, if the quark masses are small compared to the confinement scale these vacua have extremely long lifetimes.

The initial work by USQCD has focused on $\mathcal{N} = 1$ super Yang-Mills which represents a first step towards study of super QCD. Current simulations of $\mathcal{N} = 1$ super Yang-Mills have used domain wall fermions since this ensures that the lattice theory will automatically regain continuum supersymmetry in the continuum limit. The results of this work for gauge group SU(2) reveal a non-zero gluino condensate in the continuum limit in agreement with theoretical expectations [201, 202].

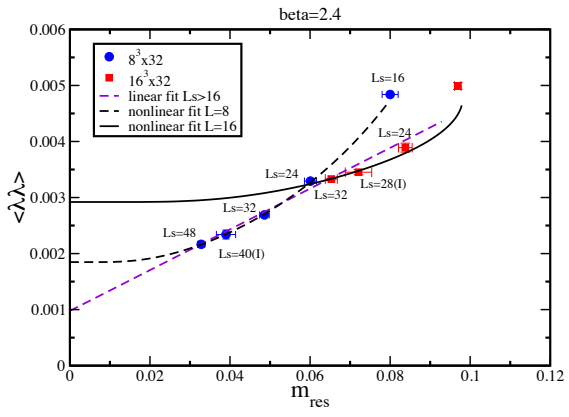

FIG. 9: Gaugino condensate vs residual mass for $SU(2)$ $\mathcal{N} = 1$ super Yang-Mills regulated usinga domain wall fermion action. The gauge coupling $\beta = 2.4$ while the bare fermion mass is set to zero. The data points correspond to different lattice volumes and L_s

In the near future we intend to extend this work to include study of the low lying spectrum of the theory which is technically more complicated since it involves the computation

of disconnected correlators. However, using stochastic estimators and dilution techniques these can be computed in a time comparable to the time needed to generate configurations. Table VI indicates the scale of resources that will be needed to compute the condensate and low lying spectrum of $\mathcal{N} = 1$ super Yang-Mills.

More importantly experience with $\mathcal{N} = 1$ super Yang-Mills will equip us to start work on the technically more challenging case of super QCD. Super QCD contains additional fields: N_f quarks and their scalar superpartners squarks and to target the interesting case of metastable vacua we will need to extend the gauge group to a larger number of colors N_c. Super QCD is also computationally more demanding; a series of DWF simulations must be performed to tune the scalar (squark) sector of the theory for a fixed value of the gauge coupling and gaugino mass [203]. The simplest system which is expected to exhibit metastable vacua corresponds to four colors and five flavors.

4. Lattice BSM resource estimates

We are currently using two choices of fermion actions for BSM physics, critically important to achieve physics goals: improved staggered fermions and domain wall fermions. However for the pseudo-Nambu-Goldstone boson project, we are developing two color gauge code using Wilson fermions both because they offer a first level project less computationally demanding than domain wall fermions, but also because we are rapidly implementing the Wilson multigrid algorithm into evolution code for both the BlueGene and GPU clusters with substantial cost reduction. Similar multigrid procedures for domain wall code is under active study [204]. For each subfield, we pick a project that is in our current plans for the next few years years, although with the rapid experimental and theoretical developments in BSM physics priorities should clearly be reevaluated beyond this time frame. Because these are preliminary investigations of theoretical possibilities, these resource estimates are smaller than in our other subfields. However, should experiment guide us into focusing more serious efforts in one of these directions, the resources needed for the investigations will be just as large as in the other subfields.

III. HARDWARE REQUIREMENTS

To reach the scientific objectives set out in Section II will require both access to the DOE's leadership class computers and the acquisition of computers dedicated to the study of QCD. The purpose of this proposal is to obtain funds to acquire and operate dedicated machines. We currently have allocations on DOE's leadership class computers, the Cray XK7, Titan, at the Oak Ridge Leadership Computing Facility (OLCF), and the IBM Blue Gene/Q and Blue Gene/P at the Argonne Leadership Computing Facility (ALCF), through the DOE's INCITE Program. We plan to request renewal of these allocations when they expire, although we understand that the Blue Gene/P will be decommissioned in the near future. Because there is close coupling between the work to be done on the two types of computers, we describe our plans for both here.

Lattice QCD calculations proceed in two steps. In the first one performs Monte Carlo calculations to generate gauge configurations with a probability proportional to their weight

(A) Resource estimates of the near-conformal BSM project				
lattice spacing a (in fermi)	fermion mass (in a units)	lattice volume $V \times T$	config generation (TF-Years)	measurements (TF-Years)
2.25×10^{-5}	0.003	$64^3 \times 128$	24	72
2.25×10^{-5}	0.004	$64^3 \times 128$	20	60
2.25×10^{-5}	0.005	$64^3 \times 128$	18	54
1.75×10^{-5}	0.0023	$96^3 \times 192$	100	300
1.75×10^{-5}	0.0030	$96^3 \times 192$	90	270
1.75×10^{-5}	0.0035	$96^3 \times 192$	80	240

(B) Resource estimates of the PNGB project				
min. M_H (GeV)	lattice volume $V \times T$	MD trajectory (time units)	config generation (TF-Years)	measurements (TF-Years)
650	$32^3 \times 64$	10000	1	2
520	$40^3 \times 80$	10000	9	12
433	$48^3 \times 96$	10000	44	60
371	$56^3 \times 112$	10000	180	270

(C) Resource estimates of the SUSY project				
lattice volume $V \times T$	wall separation L_s	bare coupling $\beta = 4/g_0^2$	trajectory. (time units)	config generation (TF-Years)
$16^3 \times 32$	24	2.4	10000	5
$16^3 \times 32$	48	2.4	10000	11
$24^3 \times 48$	24	2.4	10000	42
$24^3 \times 48$	48	2.4	10000	84
$32^3 \times 64$	24	2.4	10000	171
$32^3 \times 64$	24	2.45	10000	342
$32^3 \times 64$	48	2.45	10000	380

Total BSM resource estimate	2,941

TABLE VI: **(A)** Requested resources for the SU(3) two flavor sextet project. The fourth column shows the resources needed to generate 2,000 configurations from 20,000 MD time units. The fifth column shows the required resources for all the physics measurements. **(B)** Resources to generate gauge configuration ensembles in SU(2) gauge theory with $N_f = 2$ fermions in the fundamental representation. The inverse lattice spacing is held fixed at $a^{-1} = 5$ TeV. The first column gives the minimum Higgs mass that can fit in the volume assuming $LM_H \geq 4$ and the second column gives the corresponding lattice volume. The fourth column gives the resources in teraflop/s-years (TF-Years) needed to generate 10,000 molecular dynamics time units (1,000 equilibrated gauge configurations) for each ensemble for the Wilson fermions. **(C)** Resources needed for DWF simulation of $SU(2)$ $\mathcal{N} = 1$ Yang-Mills theory are estimated. As in previous studies, we set the bare fermion mass $m_f = 0$ for these estimates. Residual masses fall in the range 0.02-0.1 for these values of the parameters using Shamir (non-Möbius) domain wall fermions. Using three lattice volumes, two lattice spacings and two values of L_s should allow for careful extrapolation to the chiral continuum limit while maintaining control over finite volume effects.

in the Feynman path integrals that define QCD. These configurations are stored, and in the second step they are used to calculate a wide variety of physical quantities. The same configurations are often used to study problems in high energy physics and in nuclear physics. Configuration generation is the most computationally intensive part of our work. Since it involves a Markov chain, it must be carried out in a small number of streams. The generation of gauge configurations with physical quark masses and small enough lattice spacings to reach the levels of accuracy discussed in Section II requires computers that enable one to apply very large numbers of processors to individual calculations. The same is true of the calculation of propagators for physical mass quarks. These two types of calculations are therefore best done on leadership class computers.

On the other hand, dedicated computers, such as those acquired under LQCD-ext, are the appropriate platforms for the aspects of our work that need large computational resources, but do not require that the full power of a leadership class computer be applied to individual jobs. Much, but not all, of the physics analysis performed on stored gauge configurations falls into this category. The total number of floating point operations used in an analysis project ordinarily equals or exceeds the number needed to generate the ensembles being analyzed, and a significant number of projects typically make use of each ensemble. However, individual analysis jobs are typically smaller, and can be run efficiently on fewer processors, than configuration generation jobs. The analyses of different configurations are independent of each other, so they can be run in parallel. For these reasons, many analysis projects are particularly well suited for dedicated hardware. Other aspects of our work that are best suited for dedicated computers are some aspects of the study of high temperature QCD, the generation of less challenging gauge configurations, the development of new algorithms, new formulations of QCD on the lattice, and other exploratory studies. Such work plays a very important role in our research, requires large computational resources, but does not require the capabilities of leadership class machines, and is therefore not appropriate for them.

The history of our field indicates that at least as much is gained by advances in algorithms as by advances in hardware technology, and we expect this trend to continue. Indeed, the introduction of the Rational Hybrid Monte Carlo (RHMC) algorithm [205] during the LQCD Project reduced the number of floating point operations needed to generate gauge configurations with light quarks by factors of four to eight compared to algorithms in use at the time. The gauge configurations we generated during the course of LQCD-ext and plan to generate during LQCD-ext II could not be produced by the proposed resources in any reasonable amount of time without the RHMC algorithm. With the advent of simulations with physical-mass light quark, the calculation of light quark propagators dominates both configuration generation and analysis. We have therefore instituted a major effort under our SciDAC grants to accelerate the calculation of light quark propagators. The potential of this work to enhance our calculations is illustrated in Fig. 10. In addition to the multigrid method shown in this figure, we are studying a variety of approaches including domain decomposition pre-conditioning and deflation. We are confident that our continued work on algorithms will significantly enhance our productivity, extending the range of science we will be able to do. Work of this type requires significant computational resources, but is not appropriate for leadership class machines.

We believe that we will do the most science by using the computers that are best suited for each phase of our work. Moreover, we cannot simply transfer all of our calculations to the leadership class centers because the call for proposals for the INCITE Program states that

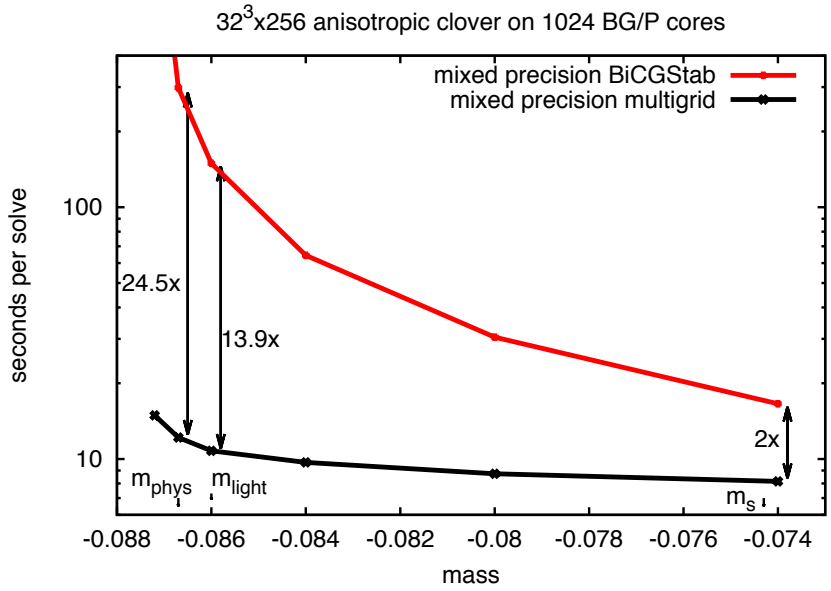

FIG. 10: The speedup in the time for the calculation of one additional Wilson-Clover quark propagator using a recently developed adaptive multigrid solver, compared with our best BiCGStab Krylov solver. This was the first successful application of multigrid to lattice QCD. Note that the gain increases with decreasing quark mass.

"Applicants must present evidence that their proposed production simulations can make effective use of a significant fraction, in most cases 20 percent or more, of the high-performance computing (HPC) systems offered for allocation." This requirement is certainly met by jobs for configuration generation and the calculation of light quark propagators, but it is not by much of our physics analysis work or our exploratory studies. A few years ago, the bulk of the floating point operations in any lattice-QCD calculation went into the generation of gauge configurations, but that is no longer so. In the 2012 USQCD allocation process, which distributed INCITE resources for calendar year 2013, five projects that received allocations were deemed appropriate for the ALCF Blue Gene/Q or the OLCF Cray XK7. These projects all involved configuration generation, and in some cases the calculation of light quark propagators. Another another five projects, which primarily involved the calculation of light quark propagators, were considered appropriate for the ALCF Blue Gene/P. The projects on these three machines received approximately half of the available USQCD resources. This was a significant jump from previous years because of the introduction of the Blue Gene/Q and the XK7, and ideally should be accompanied by an increase in dedicated resources. In the 2012 allocation process, twenty-seven projects were considered appropriate for USQCD's dedicated computers. The latter projects were critical for achieving our scientific goals.

In recent years, the largest fraction of our resource needs have been in analysis jobs, which can be run on smaller partitions of machines than configuration generation. Figure 11 shows the average core-hours used per month on the FNAL and JLab clusters in 2012 as a function of job size. The bulk of the jobs on these clusters were for physics analysis, algorithm development and exploratory projects. As can be seen, we have roughly equal needs over all scales of job size on a logarithmic plot.

[1] USQCD Collaboration web site: `http://www.usqcd.org/`.
[2] T. Blum, M. Buchoff, N. Christ, A. Kronfeld, P. Mackenzie, S. Sharpe, R. Sugar, and R. Van de Water (USQCD), Lattice QCD at the Intensity Frontier (2013).
[3] C. DeTar and F. Karsch (USQCD), Computational Challenges in QCD Thermodynamics (2013).
[4] J. Negele, D. Richards, and M. Savage (USQCD), Lattice QCD for Cold Nuclear Physics (2013).
[5] T. Appelquist, R. Brower, S. Catterall, G. Fleming, J. Giedt, A. Hasenfratz, J. Kuti, E. Neil, and D. Schaich (USQCD), Lattice Gauge Theories at the Energy Frontier (2013).
[6] A. S. Kronfeld, Annu. Rev. Nucl. Part. Sci. **62**, 265 (2012), arXiv:1203.1204 [hep-lat].
[7] C. Aubin *et al.* (Fermilab Lattice, MILC, and HPQCD), Phys. Rev. Lett. **95**, 122002 (2005), arXiv:hep-lat/0506030 [hep-lat].
[8] C. Aubin *et al.* (Fermilab Lattice, MILC, and HPQCD), Phys. Rev. Lett. **94**, 011601 (2005), arXiv:hep-ph/0408306 [hep-ph].
[9] I. F. Allison *et al.* (HPQCD and Fermilab Lattice), Phys. Rev. Lett. **94**, 172001 (2005), arXiv:hep-lat/0411027.
[10] A. Gray *et al.* (HPQCD), Phys. Rev. **D72**, 094507 (2005), arXiv:hep-lat/0507013.
[11] C. Bernard *et al.* (Fermilab Lattice and MILC), Phys. Rev. **D80**, 034026 (2009), arXiv:0906.2498 [hep-lat].
[12] D. Besson *et al.* (CLEO), Phys. Rev. **D80**, 032005 (2009), arXiv:0906.2983 [hep-ex].
[13] J. Beringer *et al.* (Particle Data Group), Phys. Rev. **D86**, 010001 (2012).
[14] S. Bethke, G. Dissertori, and G. Salam (2012) in Ref. [13].
[15] A. Manohar and C. T. Sachrajda (2012) in Ref. [13].
[16] C. T. H. Davies *et al.* (HPQCD), Phys. Rev. **D78**, 114507 (2008), arXiv:0807.1687 [hep-lat].
[17] K. Maltman, D. Leinweber, P. Moran, and A. Sternbeck, Phys. Rev. **D78**, 114504 (2008), arXiv:0807.2020 [hep-lat].
[18] S. Aoki *et al.* (PACS-CS), JHEP **10**, 053 (2009), arXiv:0906.3906 [hep-lat].
[19] E. Shintani *et al.* (JLQCD), Phys. Rev. **D82**, 074505 (2010), arXiv:1002.0371 [hep-lat].
[20] C. McNeile, C. T. H. Davies, E. Follana, K. Hornbostel, and G. P. Lepage (HPQCD), Phys. Rev. **D82**, 034512 (2010), arXiv:1004.4285 [hep-lat].
[21] C. T. H. Davies *et al.* (HPQCD), Phys. Rev. Lett. **104**, 132003 (2010), arXiv:0910.3102 [hep-ph].
[22] A. Bazavov *et al.*, Rev. Mod. Phys. **82**, 1349 (2010), arXiv:0903.3598 [hep-lat].
[23] T. Blum *et al.*, Phys. Rev. **D82**, 094508 (2010), arXiv:1006.1311 [hep-lat].
[24] S. Dürr *et al.* (BMW), Phys. Lett. **B701**, 265 (2011), arXiv:1011.2403 [hep-lat].
[25] Y. Aoki *et al.* (RBC and UKQCD), Phys. Rev. **D83**, 074508 (2011), arXiv:1011.0892 [hep-lat].
[26] A. Bazavov, T. Bhattacharya, M. Cheng, C. DeTar, H. Ding, *et al.*, Phys. Rev. **D85**, 054503 (2012), arXiv:1111.1710 [hep-lat].
[27] Y. Aoki, Z. Fodor, S. Katz, and K. Szabo, Phys. Lett. **B643**, 46 (2006), arXiv:hep-lat/0609068 [hep-lat].
[28] Y. Aoki, S. Borsanyi, S. Dürr, Z. Fodor, S. D. Katz, *et al.*, JHEP **0906**, 088 (2009).
[29] J. Dudek, R. Ent, R. Essig, K. Kumar, C. Meyer, *et al.*, Eur. Phys. J. **A48**, 187 (2012),

arXiv:1208.1244 [hep-ex].
[30] G. Isidori, Y. Nir, and G. Perez, Annu. Rev. Nucl. Part. Sci. **60**, 355 (2010), arXiv:1002.0900 [hep-ph].
[31] R. Brower *et al.* (USQCD Executive Committee), Fundamental parameters from future lattice calculations (2007).
[32] C. Bernard *et al.* (MILC), in *Chiral Dynamics 2006* (World Scientific, Singapore, 2008) arXiv:hep-lat/0611024 [hep-lat].
[33] J. Laiho, E. Lunghi, and R. S. Van de Water, Phys. Rev. **D81**, 034503 (2010), updates at `http://latticeaverages.org/`, arXiv:0910.2928 [hep-ph].
[34] G. Colangelo *et al.* (Flavianet Lattice Averaging Group), Eur. Phys. J. **C71**, 1695 (2011), arXiv:1011.4408 [hep-lat].
[35] T. Blum *et al.* (RBC and UKQCD), Phys. Rev. Lett. **108**, 141601 (2012), arXiv:1111.1699 [hep-lat].
[36] T. Blum *et al.* (RBC and UKQCD), Phys. Rev. **D86**, 074513 (2012), arXiv:1206.5142 [hep-lat].
[37] P. A. Boyle *et al.* (RBC and UKQCD), (2012), arXiv:1212.1474 [hep-lat].
[38] N. H. Christ, T. Izubuchi, C. T. Sachrajda, A. Soni, and J. Yu (RBC and UKQCD), (2012), arXiv:1212.5931 [hep-lat].
[39] A. Bazavov *et al.* (Fermilab Lattice and MILC), (2012), arXiv:1212.4993 [hep-lat].
[40] R. Dowdall, C. Davies, G. Lepage, and C. McNeile, (2013), arXiv:1303.1670 [hep-lat].
[41] E. Lunghi and A. Soni, Phys. Lett. **B697**, 323 (2011), arXiv:1010.6069 [hep-ph].
[42] J. P. Lees *et al.* (BaBar), Phys. Rev. Lett. **109**, 101802 (2012), arXiv:1205.5442 [hep-ex].
[43] J. A. Bailey *et al.* (Fermilab Lattice and MILC), Phys. Rev. Lett. **109**, 071802 (2012), arXiv:1206.4992 [hep-ph].
[44] E. D. Freeland *et al.* (Fermilab Lattice and MILC), (2012), arXiv:1212.5470 [hep-lat].
[45] P. A. Boyle, N. Garron, and R. J. Hudspith (RBC and UKQCD), Phys. Rev. **D86**, 054028 (2012), arXiv:1206.5737 [hep-lat].
[46] J. A. Bailey, T. Bae, Y.-C. Jang, H. Jeong, C. Jung, *et al.* (SWME), (2012), arXiv:1211.1101 [hep-lat].
[47] R. Zhou *et al.* (Fermilab Lattice and MILC), (2012), arXiv:1211.1390 [hep-lat].
[48] R. Zhou, (2013), arXiv:1301.0666 [hep-lat].
[49] W. Detmold, C.-J. D. Lin, S. Meinel, and M. Wingate, (2012), arXiv:1212.4827 [hep-lat].
[50] M. Lüscher, Commun. Math. Phys. **105**, 153 (1986).
[51] L. Lellouch and M. Lüscher, Commun. Math. Phys. **219**, 31 (2001), hep-lat/0003023.
[52] N. H. Christ (RBC and UKQCD), PoS **LATTICE2010**, 300 (2010), arXiv:1012.6034 [hep-lat].
[53] N. H. Christ (RBC and UKQCD), PoS **LATTICE2011**, 277 (2011), arXiv:1201.2065 [hep-lat].
[54] T. Blum *et al.* (RBC and UKQCD), Phys. Rev. **D84**, 114503 (2011), arXiv:1106.2714 [hep-lat].
[55] J. Brod and M. Gorbahn, Phys.Rev.Lett. **108**, 121801 (2012), arXiv:1108.2036 [hep-ph].
[56] M. T. Hansen and S. R. Sharpe, Phys. Rev. **D86**, 016007 (2012), arXiv:1204.0826 [hep-lat].
[57] J. L. Hewett *et al.*, *Fundamental Physics at the Intensity Frontier* (2012) arXiv:1205.2671 [hep-ex].
[58] T. Aoyama, M. Hayakawa, T. Kinoshita, and M. Nio, Phys. Rev. Lett. **109**, 111808 (2012), arXiv:1205.5370 [hep-ph].

[59] M. Davier, A. Höcker, B. Malaescu, and Z. Zhang, Eur. Phys. J. **C71**, 1515 (2011), arXiv:1010.4180 [hep-ph].
[60] K. Hagiwara, R. Liao, A. D. Martin, D. Nomura, and T. Teubner, J. Phys. **G38**, 085003 (2011), arXiv:1105.3149 [hep-ph].
[61] G. W. Bennett *et al.* (Muon $g-2$), Phys. Rev. **D73**, 072003 (2006), arXiv:hep-ex/0602035.
[62] T. Blum, Phys. Rev. Lett. **91**, 052001 (2003), arXiv:hep-lat/0212018.
[63] M. Göckeler *et al.* (QCDSF), Nucl. Phys. **B688**, 135 (2004), arXiv:hep-lat/0312032.
[64] C. Aubin and T. Blum, Phys. Rev. **D75**, 114502 (2007), arXiv:hep-lat/0608011.
[65] X. Feng, K. Jansen, M. Petschlies, and D. B. Renner (ETM), Phys. Rev. Lett. **107**, 081802 (2011), arXiv:1103.4818 [hep-lat].
[66] P. Boyle, L. Del Debbio, E. Kerrane, and J. Zanotti, Phys. Rev. **D85**, 074504 (2012), arXiv:1107.1497 [hep-lat].
[67] M. Della Morte, B. Jäger, A. Jüttner, and H. Wittig, JHEP **1203**, 055 (2012), arXiv:1112.2894 [hep-lat].
[68] C. Aubin, T. Blum, M. Golterman, and S. Peris, Phys. Rev. **D86**, 054509 (2012), arXiv:1205.3695 [hep-lat].
[69] T. Blum, T. Izubuchi, and E. Shintani, (2012), arXiv:1208.4349 [hep-lat].
[70] X. Feng, G. Hotzel, K. Jansen, M. Petschlies, and D. B. Renner, (2012), arXiv:1211.0828 [hep-lat].
[71] J. Prades, E. de Rafael, and A. Vainshtein, (2009), arXiv:0901.0306 [hep-ph].
[72] A. Nyffeler, Phys. Rev. **D79**, 073012 (2009), arXiv:0901.1172 [hep-ph].
[73] Institute for Nuclear Theory Workshop (February 28–March 4, 2011).
[74] T. S. Kosmas and J. D. Vergados, Phys. Rept. **264**, 251 (1996), arXiv:nucl-th/9408011 [nucl-th].
[75] V. Cirigliano, R. Kitano, Y. Okada, and P. Tuzon, Phys. Rev. **D80**, 013002 (2009), arXiv:0904.0957 [hep-ph].
[76] R. D. Young and A. W. Thomas, Phys. Rev. **D81**, 014503 (2010), arXiv:0901.3310 [hep-lat].
[77] D. Toussaint and W. Freeman (MILC), Phys. Rev. Lett. **103**, 122002 (2009), arXiv:0905.2432 [hep-lat].
[78] S. Dürr *et al.* (BMW Collaboration), Phys. Rev. **D85**, 014509 (2012), arXiv:1109.4265 [hep-lat].
[79] R. Horsley *et al.* (QCDSF and UKQCD Collaborations), Phys. Rev. **D85**, 034506 (2012), arXiv:1110.4971 [hep-lat].
[80] S. Dinter *et al.* (ETM Collaboration), JHEP **1208**, 037 (2012), arXiv:1202.1480 [hep-lat].
[81] H. Ohki *et al.* (JLQCD Collaboration), Phys. Rev. **D87**, 034509 (2013), arXiv:1208.4185 [hep-lat].
[82] M. Engelhardt, (2012), arXiv:1210.0025 [hep-lat].
[83] W. Freeman and D. Toussaint (MILC), (2012), arXiv:1204.3866 [hep-lat].
[84] P. E. Shanahan, A. W. Thomas, and R. D. Young, Phys. Rev. **D87**, 074503 (2013), arXiv:1205.5365 [nucl-th].
[85] P. Junnarkar and A. Walker-Loud, (2013), arXiv:1301.1114 [hep-lat].
[86] M. Gong *et al.* (χQCD Collaboration), "Strangeness and charm content of nucleon from overlap fermions on 2+1-flavor domain-wall fermion configurations," (2013), arXiv:1304.1194 [hep-ph].
[87] C. H. Llewellyn Smith, Phys. Rept. **3**, 261 (1972).
[88] J. Arrington, C. D. Roberts, and J. M. Zanotti, J. Phys. **G34**, S23 (2007),

arXiv:nucl-th/0611050 [nucl-th].
[89] A. A. Aguilar-Arevalo *et al.* (MiniBooNE Collaboration), Phys. Rev. **D81**, 092005 (2010), arXiv:1002.2680 [hep-ex].
[90] B. Bhattacharya, R. J. Hill, and G. Paz, Phys. Rev. **D84**, 073006 (2011), arXiv:1108.0423 [hep-ph].
[91] M. Day and K. S. McFarland, Phys. Rev. **D86**, 053003 (2012), arXiv:1206.6745 [hep-ph].
[92] P. Coloma, P. Huber, J. Kopp, and W. Winter, Phys. Rev. **D87**, 033004 (2013), arXiv:1209.5973 [hep-ph].
[93] A. A. Khan *et al.*, Phys. Rev. **D74**, 094508 (2006), arXiv:hep-lat/0603028.
[94] T. Yamazaki *et al.*, Phys. Rev. **D79**, 114505 (2009), arXiv:0904.2039 [hep-lat].
[95] J. D. Bratt *et al.* (LHPC), Phys. Rev. **D82**, 094502 (2010), arXiv:1001.3620 [hep-lat].
[96] C. Alexandrou *et al.* (ETM Collaboration), Phys. Rev. **D83**, 045010 (2011), arXiv:1012.0857 [hep-lat].
[97] S. Capitani, M. Della Morte, G. von Hippel, B. Jager, A. Juttner, *et al.*, Phys. Rev. **D86**, 074502 (2012), arXiv:1205.0180 [hep-lat].
[98] R. Horsley, Y. Nakamura, A. Nobile, P. Rakow, G. Schierholz, *et al.*, (2013), arXiv:1302.2233 [hep-lat].
[99] Y. Aoki *et al.* (RBC and UKQCD), Phys. Rev. **D78**, 054505 (2008), arXiv:0806.1031 [hep-lat].
[100] M. I. Buchoff, C. Schroeder, and J. Wasem, (2012), arXiv:1207.3832 [hep-lat].
[101] E. Shintani, S. Aoki, and Y. Kuramashi, Phys. Rev. **D78**, 014503 (2008), arXiv:0803.0797 [hep-lat].
[102] T. Bhattacharya, V. Cirigliano, and R. Gupta, PoS **LATTICE2012**, 179 (2012), arXiv:1212.4918 [hep-lat].
[103] R. Babich *et al.*, Phys. Rev. **D85**, 054510 (2012), arXiv:1012.0562 [hep-lat].
[104] G. S. Bali *et al.* (QCDSF), Phys. Rev. Lett. **108**, 222001 (2012), arXiv:1112.3354 [hep-lat].
[105] A. Denner, S. Heinemeyer, I. Puljak, D. Rebuzzi, and M. Spira, Eur. Phys. J. **C71**, 1753 (2011), arXiv:1107.5909 [hep-ph].
[106] S. Heinemeyer *et al.* (LHC Higgs Cross Section Working Group), (2013), 10.5170/CERN-2013-004, arXiv:1307.1347 [hep-ph].
[107] I. Allison *et al.* (HPQCD Collaboration), Phys.Rev. **D78**, 054513 (2008), arXiv:0805.2999 [hep-lat].
[108] K. G. Chetyrkin *et al.*, Phys. Rev. **D80**, 074010 (2009), arXiv:0907.2110 [hep-ph].
[109] D. B. Kaplan, Phys. Lett. **B288**, 342 (1992), arXiv:hep-lat/9206013 [hep-lat].
[110] V. Furman and Y. Shamir, Nucl. Phys. **B439**, 54 (1995), arXiv:hep-lat/9405004 [hep-lat].
[111] P. M. Vranas, Phys. Rev. **D74**, 034512 (2006), arXiv:hep-lat/0606014 [hep-lat].
[112] E. Follana *et al.* (HPQCD), Phys. Rev. **D75**, 054502 (2007), arXiv:hep-lat/0610092 [hep-lat].
[113] J. R. Green *et al.*, (2012), arXiv:1209.1687 [hep-lat].
[114] A. Airapetian *et al.* (HERMES), Phys. Rev. **D75**, 012007 (2007), arXiv:hep-ex/0609039.
[115] P. Hagler *et al.* (LHPC), Phys. Rev. **D77**, 094502 (2008), arXiv:0705.4295 [hep-lat].
[116] S. N. Syritsyn *et al.*, PoS **LATTICE2011**, 178 (2011), arXiv:1111.0718 [hep-lat].
[117] D. Brommel *et al.* (QCDSF-UKQCD), PoS **LAT2007**, 158 (2007), arXiv:0710.1534 [hep-lat].
[118] R. G. Edwards, J. J. Dudek, D. G. Richards, and S. J. Wallace, Phys. Rev. **D84**, 074508 (2011), arXiv:1104.5152 [hep-ph].

[119] M. Lüscher, Nucl. Phys. **B354**, 531 (1991).
[120] J. J. Dudek, R. G. Edwards, and C. E. Thomas, Phys. Rev. **D87**, 034505 (2013), arXiv:1212.0830 [hep-ph].
[121] C. Liu, X. Feng, and S. He, Int. J. Mod. Phys. **A21**, 847 (2006), arXiv:hep-lat/0508022 [hep-lat].
[122] M. Döring, U.-G. Meissner, E. Oset, and A. Rusetsky, Eur. Phys. J. **A47**, 139 (2011), arXiv:1107.3988 [hep-lat].
[123] S. Aoki *et al.* (HAL QCD Collaboration), Proc. Japan Acad. **B87**, 509 (2011), arXiv:1106.2281 [hep-lat].
[124] R. A. Briceno and Z. Davoudi, (2012), arXiv:1204.1110 [hep-lat].
[125] P. Guo, J. Dudek, R. Edwards, and A. P. Szczepaniak, (2012), arXiv:1211.0929 [hep-lat].
[126] S. R. Beane, P. F. Bedaque, K. Orginos, and M. J. Savage, Phys. Rev. Lett. **97**, 012001 (2006), arXiv:hep-lat/0602010.
[127] S. R. Beane *et al.* (NPLQCD), Phys. Rev. **D81**, 054505 (2010), arXiv:0912.4243 [hep-lat].
[128] S. R. Beane *et al.* (NPLQCD), Phys. Rev. Lett. **106**, 162001 (2011), arXiv:1012.3812 [hep-lat].
[129] S. R. Beane *et al.* (NPLQCD), Phys. Rev. **D85**, 054511 (2012), arXiv:1109.2889 [hep-lat].
[130] S. R. Beane *et al.*, (2012), arXiv:1206.5219 [hep-lat].
[131] S. R. Beane *et al.*, (2013), arXiv:1301.5790 [hep-lat].
[132] S. Aoki, T. Hatsuda, and N. Ishii, Comput. Sci. Dis. **1**, 015009 (2008), arXiv:0805.2462 [hep-ph].
[133] S. Aoki, T. Hatsuda, and N. Ishii, Prog. Theor. Phys. **123**, 89 (2010), arXiv:0909.5585 [hep-lat].
[134] N. Ishii, S. Aoki, and T. Hatsuda, Phys. Rev. Lett. **99**, 022001 (2007), arXiv:nucl-th/0611096.
[135] T. Yamazaki, K.-i. Ishikawa, Y. Kuramashi, and A. Ukawa, Phys. Rev. **D86**, 074514 (2012), arXiv:1207.4277 [hep-lat].
[136] T. Inoue *et al.* (HAL QCD), Phys. Rev. Lett. **106**, 162002 (2011), arXiv:1012.5928 [hep-lat].
[137] W. Detmold and K. Orginos, (2012), arXiv:1207.1452 [hep-lat].
[138] M. Della Morte, B. Jager, H. Wittig, and A. Juttner, PoS **LATTICE2011**, 161 (2011), arXiv:1111.2193 [hep-lat].
[139] F. Berruto, T. Blum, K. Orginos, and A. Soni, Phys. Rev. **D73**, 054509 (2006), arXiv:hep-lat/0512004.
[140] S. Aoki *et al.*, (2008), arXiv:0808.1428 [hep-lat].
[141] J. Wasem, Phys. Rev. **C85**, 022501 (2012), [PoS Lattice2011:179,2011], arXiv:1108.1151 [hep-lat].
[142] M. T. Gericke *et al.*, Phys. Rev. **C83**, 015505 (2011).
[143] I. Arsene *et al.* (BRAHMS Collaboration), Nucl. Phys. **A757**, 1 (2005).
[144] B. Back, M. Baker, M. Ballintijn, D. Barton, B. Becker, *et al.*, Nucl. Phys. **A757**, 28 (2005).
[145] J. Adams *et al.* (STAR Collaboration), Nucl. Phys. **A757**, 102 (2005).
[146] K. Adcox *et al.* (PHENIX Collaboration), Nucl. Phys. **A757**, 184 (2005).
[147] B. V. Jacak and B. Müller, Science **337**, 310 (2012).
[148] M. Aggarwal *et al.* (STAR Collaboration), arXiv: 1007.2613 [nucl-ex] (2010).
[149] G. Odyniec, Acta Phys. Polon. **B43**, 627 (2012).
[150] A. Bazavov, T. Bhattacharya, M. Cheng, C. DeTar, H. Ding, *et al.*, Phys. Rev. **D85**, 054503 (2012).

[151] M. Aggarwal *et al.* (STAR Collaboration), Phys. Rev. **C83**, 034910 (2011).
[152] O. Kaczmarek, F. Karsch, E. Laermann, C. Miao, S. Mukherjee, *et al.*, Phys. Rev. **D83**, 014504 (2011).
[153] A. Bazavov, H. Ding, P. Hegde, O. Kaczmarek, F. Karsch, *et al.*, Phys. Rev. Lett. **109**, 192302 (2012).
[154] M. A. Stephanov, K. Rajagopal, and E. V. Shuryak, Phys. Rev. Lett. **81**, 4816 (1998).
[155] S. Ejiri, F. Karsch, and K. Redlich, Phys. Lett. **B633**, 275 (2006).
[156] M. Cheng, P. Hendge, C. Jung, F. Karsch, O. Kaczmarek, *et al.*, Phys. Rev. **D79**, 074505 (2009).
[157] C. Allton, M. Döring, S. Ejiri, S. Hands, O. Kaczmarek, *et al.*, Phys. Rev. **D71**, 054508 (2005).
[158] R. Gavai and S. Gupta, Phys. Rev. **D71**, 114014 (2005).
[159] V. Koch, (2008), arXiv:0810.2520 [nucl-th].
[160] M. Aggarwal *et al.* (STAR Collaboration), Phys. Rev. Lett. **105**, 022302 (2010).
[161] X. Luo (STAR Collaboration), arXiv:1210.5573 [nucl-ex] (2012).
[162] J. Mitchell (PHENIX Collaboration), arXiv:1210.5573 [nucl-ex] (2012).
[163] S. Borsanyi, arXiv: 1210.6901 [hep-lat] (2012).
[164] S. Ejiri, F. Karsch, E. Laermann, C. Miao, S. Mukherjee, *et al.*, Phys. Rev. **D80**, 094505 (2009).
[165] S. Aoki, H. Fukaya, and Y. Taniguchi, Phys. Rev. **D86**, 114512 (2012).
[166] R. D. Pisarski and F. Wilczek, Phys. Rev. **D29**, 338 (1984).
[167] T. Hatsuda, M. Tachibana, N. Yamamoto, and G. Baym, Phys. Rev. Lett. **97**, 122001 (2006).
[168] M. Cheng, N. H. Christ, M. Li, R. D. Mawhinney, D. Renfrew, *et al.*, Phys. Rev. **D81**, 054510 (2010).
[169] A. Bazavov *et al.* (HotQCD Collaboration), Phys. Rev. **D86**, 094503 (2012).
[170] H. Ding, A. Francis, O. Kaczmarek, F. Karsch, H. Satz, *et al.*, Phys. Rev. **D86**, 014509 (2012).
[171] M. Asakawa, T. Hatsuda, and Y. Nakahara, Prog. Part. Nucl. Phys. **46**, 459 (2001).
[172] H.-T. Ding, arXiv: 1210.5442 [nucl-th] (2012).
[173] G. Aarts, C. Allton, S. Kim, M. Lombardo, M. Oktay, *et al.*, JHEP **1111**, 103 (2011).
[174] H.-T. Ding, A. Francis, O. Kaczmarek, F. Karsch, E. Laermann, *et al.*, Phys. Rev. **D83**, 034504 (2011).
[175] S. Chatrchyan *et al.* (CMS Collaboration), Phys. Lett. **B716**, 30 (2012), arXiv:1207.7235 [hep-ex].
[176] G. Aad *et al.* (ATLAS Collaboration), Phys. Lett. **B716**, 1 (2012), arXiv:1207.7214 [hep-ex].
[177] S. Weinberg, Phys. Rev. **D19**, 1277 (1979).
[178] L. Susskind, Phys. Rev. **D20**, 2619 (1979).
[179] T. Banks and A. Zaks, Nucl. Phys. **B196**, 189 (1982).
[180] W. A. Bardeen, C. N. Leung, and S. Love, Phys. Rev. Lett. **56**, 1230 (1986).
[181] W. D. Goldberger, B. Grinstein, and W. Skiba, Phys. Rev. Lett. **100**, 111802 (2008), arXiv:0708.1463 [hep-ph].
[182] N. Arkani-Hamed, A. G. Cohen, and H. Georgi, Phys. Lett. **B513**, 232 (2001), arXiv:hep-ph/0105239 [hep-ph].
[183] N. Arkani-Hamed, A. Cohen, E. Katz, A. Nelson, T. Gregoire, *et al.*, JHEP **0208**, 021

(2002), arXiv:hep-ph/0206020 [hep-ph].
[184] N. Arkani-Hamed, A. Cohen, E. Katz, and A. Nelson, JHEP **0207**, 034 (2002), arXiv:hep-ph/0206021 [hep-ph].
[185] D. B. Kaplan and H. Georgi, Phys. Lett. **B136**, 183 (1984).
[186] D. B. Kaplan, H. Georgi, and S. Dimopoulos, Phys. Lett. **B136**, 187 (1984).
[187] H. Georgi and D. B. Kaplan, Phys. Lett. **B145**, 216 (1984).
[188] J. Thaler, JHEP **0507**, 024 (2005), arXiv:hep-ph/0502175 [hep-ph].
[189] M. Schmaltz and J. Thaler, JHEP **0903**, 137 (2009), arXiv:0812.2477 [hep-ph].
[190] T. Appelquist and Y. Bai, Phys. Rev. **D82**, 071701 (2010), arXiv:1006.4375 [hep-ph].
[191] R. Foadi, M. T. Frandsen, and F. Sannino, (2012), arXiv:1211.1083 [hep-ph].
[192] T. Appelquist, G. T. Fleming, and E. T. Neil, Phys. Rev. Lett. **100**, 171607 (2008), arXiv:0712.0609 [hep-ph].
[193] A. Cheng, A. Hasenfratz, and D. Schaich, Phys. Rev. **D85**, 094509 (2012), arXiv:1111.2317.
[194] Z. Fodor, K. Holland, J. Kuti, D. Nogradi, C. Schroeder, *et al.*, Phys. Lett. **B718**, 657 (2012), arXiv:1209.0391 [hep-lat].
[195] J. Kogut and D. Sinclair, Phys. Rev. **D84**, 074504 (2011), arXiv:1105.3749 [hep-lat].
[196] M. E. Peskin, Nucl. Phys. **B175**, 197 (1980).
[197] M. Schmaltz and D. Tucker-Smith, Annu. Rev. Nucl. Part. Sci. **55**, 229 (2005), arXiv:hep-ph/0502182 [hep-ph].
[198] E. Katz, J.-y. Lee, A. E. Nelson, and D. G. Walker, JHEP **0510**, 088 (2005), arXiv:hep-ph/0312287 [hep-ph].
[199] J. Galloway, J. A. Evans, M. A. Luty, and R. A. Tacchi, JHEP **1010**, 086 (2010), arXiv:1001.1361 [hep-ph].
[200] K. A. Intriligator, N. Seiberg, and D. Shih, JHEP **04**, 021 (2006), arXiv:hep-th/0602239.
[201] J. Giedt, R. Brower, S. Catterall, G. T. Fleming, and P. Vranas, Phys. Rev. **D79**, 025015 (2009), arXiv:0810.5746 [hep-lat].
[202] M. G. Endres, Phys. Rev. **D79**, 094503 (2009), arXiv:0902.4267 [hep-lat].
[203] J. W. Elliott, J. Giedt, and G. D. Moore, Phys. Rev. **D78**, 081701 (2008), arXiv:0806.0013 [hep-lat].
[204] S. D. Cohen, R. Brower, M. Clark, and J. Osborn, PoS **LATTICE2011**, 030 (2011), arXiv:1205.2933 [hep-lat].
[205] M. Clark and A. Kennedy, Phys. Rev. Lett. **98**, 051601 (2007), arXiv:hep-lat/0608015 [hep-lat].